

Nanoscale heterostructures for Photocatalysis & Photovoltaics



**A Thesis Submitted For Partial Fulfillment
Of BS – MS Dual Degree Programme**

By

T.SRIHARSHA

Under the Guidance of

Prof. Aninda J. Bhattacharyya

Solid state and Structural Chemistry Unit

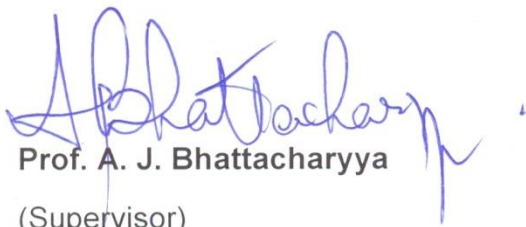
INDIAN INSTITUTE OF SCIENCE – Bangalore

Indian Institute of Science Education and Research

Pune

Certificate

This is to certify that this thesis entitled “**Nanoscale heterostructures for Photocatalysis and Photovoltaics**” towards the partial fulfillment of the BS-MS dual degree programme at the Indian Institute of Science Education and Research, Pune, represents original research carried out by **T.SRIHARSHA** at **Indian Institute of Science, Bangalore** under the supervision of **Prof. Aninda J. Bhattacharyya, SSCU** during the academic year 2014-2015.



Prof. A. J. Bhattacharyya

(Supervisor)

Date: 25.03.2015.

Place: BANGALORE.

Declaration

I declare that the matter embodied in the report entitled “**Nanoscale heterostructures for Photocatalysis and Photovoltaics**” are the results of the experiments and investigations carried out by me during the academic year 2014-2015 at Solid state and Structural Chemistry Unit, Indian Institute of Science, Bangalore, under the supervision of **Prof. Aninda J. Bhattacharyya** and the same has not been submitted elsewhere for any other degree, in any other University.



T.SRIHARSHA

Date: 25/02/2015

Place: Bangalore

Acknowledgements

I would like to express my gratitude to Professor Aninda J. Bhattacharyya for his continuous support and creating an ambience of enthusiasm, and providing me with the required freedom during my tenure as a project student.

I would also like to thank Dr. Nirmalya Ballav for morally supporting me and inspiring me to achieve excellence in science. He has been a great support for me during my course work. His fantabulous teaching skills really helped me to understand core concepts of the subject.

I would like to thank Mr. Tamilselvan Muthusamy for patiently guiding me in what has been an enriching and productive journey and for introducing me to various laboratory techniques and instruments. I would also like to thank Mr. Sayantan Mazumdar, Dr. Dipak Dutta, Mr. Suman Das, Ms. Subhra Gope, Ms. Sudeshna Sen, Mr. Rudra N. Samajder, Ms. Sneha Malunavar and Mr. Santhosha AL for helping me out throughout this period of my project and maintaining a lively and cheerful atmosphere in the lab. I thank my friend Arani Biswas for all the laughter, company and football.

I would also like to thank my parents and my sis for being a constant support throughout. Finally, I would like to thank my closest friends without whom the past would not be as good as it has been.

-Sriharsha

Contents	Page number
• Abstract.....	8
• Introduction.....	9
• Chapter 1: Heterostructured Sn ₃ O ₄ /Cu ₂ O for investigating degradation profile of an organic pollutant in different conditions	
1. Experimental procedure.....	14
2. Characterization.....	16
3. Results and discussion.....	17
4. Conclusion.....	28
• Chapter 2:	
1. Synthesis of SnS ₂ nanoflakes and its Photocatalysis	
i. Experimental procedure.....	29
ii. Results and discussion.....	30
2. SnS ₂ /KNbO ₃ heterostructure for enhance photocatalytic activity	
i. Experimental procedure.....	38
ii. Results and discussion.....	40
3. Conclusions.....	47
• References.....	48

List of Figures	Page number
Figure 1: Different types of heterojunctions.....	10
Figure 2: Illustration of electron transfer between two semiconductors.....	11
Figure 3: Spectrum of metal halide lamp.....	13
Figure 4: Powder XRD diffractogram of Sn ₃ O ₄	18
Figure 5: Powder XRD diffractogram of Cu ₂ O.....	18
Figure 6: Powder XRD diffractogram of Sn ₃ O ₄ /Cu ₂ O at different concentrations.....	19
Figure 7: SEM images of Sn ₃ O ₄ & Cu ₂ O.....	20
Figure 8: SEM images of Sn ₃ O ₄ /Cu ₂ O heterostructure.....	21
Figure 9: UV Vis diffuse reflectance spectrum of Sn ₃ O ₄ & Cu ₂ O.....	22
Figure 10: Plot for estimation of bandgap of Sn ₃ O ₄ & Cu ₂ O.....	22
Figure 11: UV Vis diffuse reflectance spectrum of Sn ₃ O ₄ /Cu ₂ O.....	23
Figure 12: Schematic diagram for energy band structure.....	24
Figure 13: pH vs. Zeta potential of Sn ₃ O ₄ & Sn ₃ O ₄ /Cu ₂ O.....	25
Figure 14: Degradation profile of IC by Sn ₃ O ₄ /Cu ₂ O.....	26
Figure 15: Degradation profile of IC by Sn ₃ O ₄ /Cu ₂ O at different pH.....	27
Figure 16: UV Vis spectrum of decomposition of IC by Sn ₃ O ₄ /Cu ₂ O.....	27
Figure 17: Powder XRD diffractogram of SnS ₂	32
Figure 18: SEM images of SnS ₂	32
Figure 19: UV Vis Diffuse reflectance spectrum of SnS ₂	33
Figure 20: Plot for estimating the bandgap of SnS ₂	34
Figure 21: pH vs. Zeta potential of SnS ₂	34
Figure 22: Degradation profiles of IC by SnS ₂	36
Figure 23: UV Vis spectrum of decomposition of IC by SnS ₂	36
Figure 24: Proposed band configuration of NiO, KNbO ₃ and SnS ₂	37

Figure 25: Powder XRD diffractogram of KNbO_3	40
Figure 26: Powder XRD diffractogram of $\text{SnS}_2/\text{KNbO}_3$	41
Figure 27: SEM images of KNbO_3	42
Figure 28: SEM images of $\text{SnS}_2/\text{KNbO}_3$	43
Figure 29: UV Vis diffuse reflectance spectrum of KNbO_3	44
Figure 30: UV Vis diffuse reflectance spectrum of $\text{SnS}_2/\text{KNbO}_3$	44
Figure 31: pH vs. Zeta potential of $\text{SnS}_2/\text{KNbO}_3$	45
Figure 32: Degradation profiles of IC by $\text{SnS}_2/\text{KNbO}_3$	46

List of Tables

Page number

Table 1: Detailed elemental composition of Sn_3O_4 , Cu_2O & $\text{Sn}_3\text{O}_4/\text{Cu}_2\text{O}$	20
Table 2: Detailed elemental composition of KNbO_3 & $\text{SnS}_2/\text{KNbO}_3$	42

Abstract

Different metal oxides/sulphides were chosen and presented, to enhance the degradation of organic pollutants under visible light irradiation. Novel heterostructured photocatalysts were fabricated *via* facile hydrothermal and solution phase route. The serendipitous $\text{Sn}_3\text{O}_4/\text{Cu}_2\text{O}$ & $\text{SnS}_2/\text{KNbO}_3$ heterostructures at various conditions exhibit remarkable potential as a visible light photocatalysts with an advantage of recyclability in comparison to their seeding precursors. In addition, the characterization, and the chemical and physical measurements focused upon magnifying the photocatalytic activity were discussed. The effectiveness of the materials was tested by investigating the degradation profiles of a model dye, Indigo carmine (IC).

Introduction

In today's world, most industrialized nations face tremendous environmental problems with regard to the disposal of hazardous wastes, contaminated groundwater, and the control of toxic air contaminants. Because of disposal of such toxic wastes, the surrounding land and groundwater have become contaminated with various chemicals such as heavy metals, solvents, halogenated hydrocarbons, fuels etc. Photocatalysis has been proven to be an effective method for the degradation of various organic molecules, amongst other uses.

As a result, the development of efficient photocatalysis techniques is desirable and paramount in environmental pollution mediation. Significant progress has been made over the past decade in the development of novel and efficient photocatalysts. These include inorganic, molecular, and hybrid organic/inorganic materials. They have been explored to meet certain specific requirements such as light-absorbing wavelength modification, photo-induced charge separation, and a faster photocatalytic reaction. Extensive research has been carried out on semiconductors as photocatalysts in the degradation of organic pollutants that are hazardous to nature and mankind and difficult to degrade by natural means.

The effectiveness of such photocatalyst nanostructures are determined by studying the degradation kinetics of organic dyes. Generally, dyes are complex unsaturated aromatic compounds with important characteristics like color, intensity, solubility, etc. In addition to their usual application as coloring agents, synthetic dyes are also utilized in technology, such as in the medical, electronics and specifically the nonimpact printing industries. For example, they are utilized in electrophotography (laser printing and photocopying) in both the organic photoconductor and the toner, in direct and thermal transfer printing, and also in ink-jet printing. [4]

Nanostructured materials when compared to bulk materials are very versatile owing to their varied electrical, mechanical, magnetic and optical properties. Such properties can be tuned by changing the morphology or by confining the dimensions of these materials so that they exhibit both surface and bulk properties. Over the years,

various advancements have been made in the areas of energy conversion and storage, electronics and optoelectronics, biomedicine etc. with the help of such nanomaterials. Among all the nanomaterials, the semiconductors nanomaterials are considered as candidates for photocatalysts, mainly chalcogenides namely, oxides and sulfides *viz.* CdS, ZnO, TiO₂, WO₃ etc. TiO₂ is one of the well-known semiconductor photocatalysts that has been extensively used for its low cost and non-toxicity. However, given its wide band-gap, TiO₂ is not very efficient in absorbing the total visible spectrum of sunlight. Although various strategies have been implemented to enhance the optical absorption of TiO₂, the photocatalytic activity is still limited. Thus, it is of utmost importance to develop proper and efficient substitutes of TiO₂ for photocatalysis.

Among these semiconductors, there are many varieties *viz.* binary oxide semiconductors, doped semiconductors, composite semiconductors and nano semiconductor heterostructures. In the recent research, there's an increasing in interest for nano semiconductor heterostructure, as coupling one semiconductor with another having a favorable energy not only improves the charge separation but also enhances the photo-electrochemical properties like the efficiency of photocatalysis & photovoltaics. These materials have presented themselves as efficient candidates in photocatalysis for uses in solar energy conversion and environmental remediation.

The main scheme of fabricating semiconductor heterojunctions depends upon the band configurations and the alignment between both the semiconductors. When two semiconductors with different Fermi levels and band positions are put together into a composite, the electrons from the semiconductor with higher Fermi level energy flows into the semiconductor with lower Fermi level creating bending of the band upward or downward. [33] Semiconductor heterojunctions are divided into three types depending on the relative energy of conduction band (CB) and valance band (VB) and the bandgap: 1) straddling type, 2) staggered type and 3) broken type as shown in Figure 1.

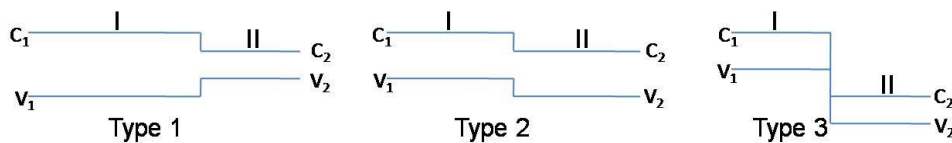


Figure 1: Different types of heterojunctions

Since the past decade, combination of two different semiconductors into a heterostructure as photocatalysts had been extensively studied because of their effective charge separation at the interfaces. [33] Particularly, for the use of H₂ generation and CO₂ reduction, for the semiconductors to form a heterostructure, they must have conduction band levels higher than the redox potential of these reactions. Semiconductor metal oxides, like TiO₂, ZnO act as base materials and couple with another semiconductor with higher conduction band level to form a heterojunction. Although, semiconductors with higher band gap are coupled with narrow bandgap semiconductors as shown in Figure 2.

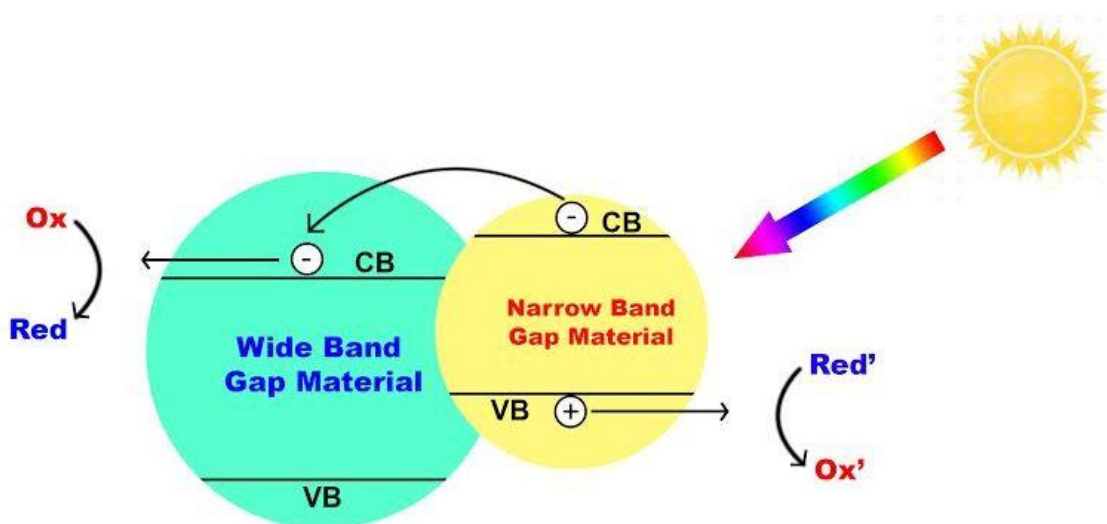


Figure 2: Illustration of electron transfer between two semiconductors

Photocatalysis:

Photocatalytic processes are quite complex since the reactions take place in the photocatalysts and at the photocatalyst-reaction mixture interface. A photocatalytic reaction comprises of several processes-

- 1. Absorption of photons by semiconductors:** The electronic structure of semiconductors comprises of a filled valence band and an empty conduction band. As a result, these materials can act as photocatalysts in photo-induced redox processes.

Upon irradiation, an electron in the valence band is excited to the conduction band leaving behind a hole.

2. Relaxation: After the initial excitation, the electron and hole move to, conduction band minimum and valence band maximum respectively.

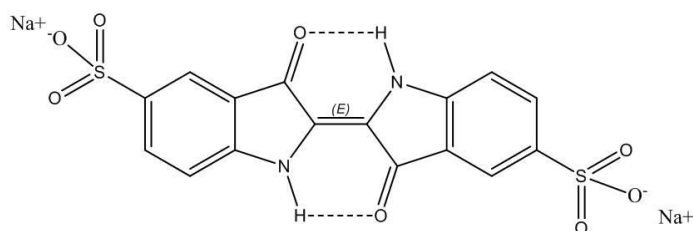
3. Recombination processes: The electron-hole pairs are a metastable species and generally tend to recombine giving off thermal energy. They can also get trapped or react with electron donors and/or acceptors adsorbed on the semiconductor surface. Presence of suitable scavengers or defect sites delay the recombination processes and thus redox reactions can take place.

4. Charge transport: During the course of the redox process, the electrons and holes migrate towards the electrodes.

5. Water absorption on the surface: The hydrophobic and hydrophilic surfaces of the photocatalyst are of paramount importance in tuning the photocatalytic efficiency.

6. Free-radical formation: Electrons from water are transferred to the photocatalysts (since holes attract electrons). Valence bond holes are powerful oxidants. Usually, organic photo degradation reactions utilize this property of the holes either directly or indirectly. However, to prevent buildup of charge, certain reducible species are also provided. [6]

pH plays a crucial role in the degradation of dyes using photocatalysts. The surface charge of photocatalysts varies with pH, it has positive charge and the anionic dyes degrade faster when $\text{pH} < \text{pH}_{\text{pzc}}$ (point zero charge). Conversely, when the surface charge is negative as in, when $\text{pH} > \text{pH}_{\text{pzc}}$ degradation of cationic dyes is most favored. pH controls the surface charge and adsorption coefficient of charged substrates. [5]



Structure of dye Indigo carmine

Indigo carmine dye ($C_{16}H_8N_2Na_2O_8S_2$) is an organic compound with a shade of dark blue. The main use of this dye is for cotton yarn and as a colorant. It is an anionic dye. [5]

In this report, we have demonstrated the efficiency of $Sn_3O_4-Cu_2O$, SnS_2 nano flakes, SnS_2-KNbO_3 , etc. nano-heterostructures in photocatalytic dye-degradation reactions and their corresponding enhanced optical absorption in the solar spectrum as compared to TiO_2 . An organic contaminant Indigo carmine was used as a probe molecule to carry out the photocatalytic experiments with as-synthesized nanomaterials under visible light irradiation at room temperature using 400 Watt metal halide lamp, which has the spectral distribution as shown in Figure 3. The degradation profiles of active materials were investigated at different pH.

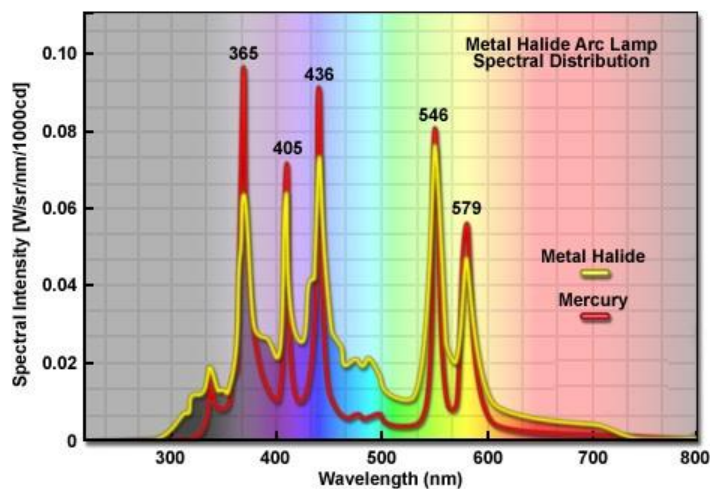


Figure 3: Spectrum of metal halide lamp (taken from <http://zeiss-campus.magnet.fsu.edu/articles/lightsources/metalhalide.html>)

Chapter 1: Heterostructured Sn_3O_4/Cu_2O for investigating degradation profile of an organic pollutant in different conditions

Since the last decade, metal oxide semiconductors were of keen interest due to their chemical stability in both acidic and basic medium. But on the contrary, in most metal oxides the wide bandgap and their ability of optical absorption falling in the range of UV light have been the disadvantages. To counterbalance these metal oxides were doped using other metals. For example, TiO_2 being a wide bandgap semiconductor, when

doped with nitrogen [34] and copper [35] show an enhanced photocatalytic activity. Tin oxides also fall in the same category of TiO_2 .

Tin oxides also have been crucial subjects of fundamentals studies over all other metal oxides. However, in this modern era these compounds play their role as prime candidates in catalysis and opto-electronic applications. In the course of time many studies have been carried out on these oxides and their non-stoichiometric intermediate compounds *viz.* SnO_2 , Sn_3O_4 , and SnO . The structure, stability and the properties of these materials are still under debate. In this report, the properties and applications of Sn_3O_4 has been discussed. Sn_3O_4 is n-type semiconductor and a multi-valence compound with Tin(II) and Tin(IV). [24]

Among all the semiconductor oxides, oxides of copper are of intensive interest and have been extensively studied. Out of the oxides of copper, cuprous oxide has been broadly investigated for its distinctive properties. Cu_2O is p-type semiconductor with a bandgap of 2 - 2.2eV. [28]

Recent advances in creating nanoscale semiconductor assemblies between two metal oxides have portended a new generation of materials in the field of photocatalysis and photovoltaics. This practice enabled coexistence of discrete physical properties into a distinctive diverse combination.

1.1 Experimental Procedure:

1.1.1 Synthesis procedure: Sn_3O_4 & Cu_2O :

Tin oxide, $(\text{Sn}^{2+})_2(\text{Sn}^{4+})\text{O}_4$ was synthesized via hydrothermal route. [27] It is a mixed-valence compound containing Stannous, which exists in more than one oxidation state. The nano crystals of stannous oxide were synthesized through hydrothermal route where Trisodium citrate was used as the surfactant. SnCl_2 (0.95 g, 5.0 mmol) and $\text{Na}_3\text{C}_6\text{H}_5\text{O}_7 \cdot 5\text{H}_2\text{O}$ (3.64 g, 10 mmol) were dissolved in 12.5 mL of deionized water and stirred for 10 min. 0.2 M NaOH was dissolved in 12.5 mL of DI water and added to the above solution while stirring continuously to attain a homogenous solution. Trisodium citrate here helps in maintaining acidic pH in the solution. This solution was then

transferred to a 40 mL Teflon vessel in a stainless steel autoclave and heated at a temperature of 180° C for 15 h. The autoclave was cooled down to room temperature and the precipitate was obtained by centrifugation. During centrifugation the precipitate was washed several times with DI water, two times with ethanol and dried at a temperature of 90° C under vacuum. The colour of the powder after drying was light yellow.

By following a reported procedure, [26] Copper acetate $\text{Cu}(\text{OAc})_2 \cdot \text{H}_2\text{O}$ (0.5 g, 2.5 mmol) was taken in 50 mL DI water and put down for vigorous stirring. After making sure that copper acetate was totally dissolved in the water, with subsequent stirring, Hydrazine hydrate $\text{N}_2\text{H}_4 \cdot \text{H}_2\text{O}$ (100 μL) was added. The mixture was additionally stirred for 20 min. The gradual change of colour blue to the colour Olive green was observed. Centrifugation of the solution was performed by washing the precipitate with DI water and ethanol for several times. The obtained product was dried at 70 °C under vacuum. Cuprous oxide is orange in colour.

Hetero-structure $\text{Sn}_3\text{O}_4\text{-Cu}_2\text{O}$

After the synthesis of Sn_3O_4 , the fabrication of heterostructures was done by following a solution phase procedure. Three different solutions were prepared by mixing Sn_3O_4 (0.25 g) in 50 mL DI water. All the three solutions were placed in the ultrasonic bath and subjected for sonication till a homogenous dispersion was observed. Three different concentrations of $\text{Cu}(\text{OAc})_2$ (0.125 g, 0.25 g and 0.5 g) were added to the above solution under vigorous stirring. Finally, $\text{N}_2\text{H}_4 \cdot \text{H}_2\text{O}$ (26 μL , 50 μL and 100 μL) were quickly put in to the respective suspensions and continued stirring for 30 min. The obtained product was washed several times with distilled water and pure ethanol and separated by centrifugation, followed by drying it at 75° C under vacuum. The colour of the acquired powder was yellow.

Chemicals used in the synthesis were of superior grade which were commercially available at Sigma Aldrich and SDL Pvt. Ltd. Chemicals were directly used without any further purification.

1.1.2 Photocatalytic experiments:

First, photocatalytic properties of the as-synthesized precursors Sn_3O_4 , Cu_2O were investigated by evaluating the degradation profiles of Indigo carmine ($\text{C}_{16}\text{H}_8\text{N}_2\text{Na}_2\text{O}_8\text{S}_2$) using a metal halide lamp. Then, taking three different solutions varying the concentrations of Cu_2O were studied, out of which the most efficient concentration was run again at different pH. pH of the solution was altered before adding the dye.

The photocatalysis experiments were implemented using an apparatus set up in our lab, including a metal halide lamp, cooling attachment to prevent overheating of the lamp by circulating cold water and a magnetic stirrer. All the experiments were performed in 30 mL glass vials at room temperature. Before irradiating, 10 mg of IC was dissolved in 10 mL of DI water to make a 1000 ppm solution and stored in a dark place. 20 mg of the active material was taken in 19 mL of DI water and an aliquot of 1 mL IC was added. Subsequently, the solution was magnetically stirred in dark for 2 h for the photocatalyst and the dye to attain adsorption/desorption equilibrium. During irradiation, 1 mL aliquots were collected from the reaction cell using a micro pipette at a 10 min interval for 120 min. The collected suspensions were subjected to centrifugation in order to separate the active material. Centrifugation was performed at high rpm (10000 rpm).

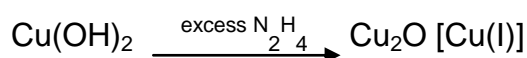
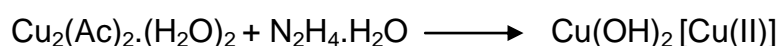
1.2 Characterization:

Powder X-ray diffraction (XRD) patterns were recorded using PANalytical- Empyrean X-ray diffractometer by $\text{Cu K}\alpha$ radiation at a scanning rate of $5^\circ/\text{min}$ for 2θ ranging from 10 to 70° . X'PertHighScore Plus was used for plotting the recorded XRD patterns. Scanning Electron Microscopy was performed using ZEISS 1550VP Field Emission SEM with Oxford EDS (Energy-Dispersive X-ray Spectroscopy) which is used in supporting the observations by identifying the elemental composition of the sample. Typically, the samples were drop casted on a silicon wafer which is framed to sample holder using conductive carbon tape. UV-Vis diffuse reflectance spectra were recorded using PerkinElmer Lambda 750 UV-Vis Infrared spectrometer with BaSO_4 as the blank. Change in pH of the solutions was monitored using EUTECH Instruments pH Tutor pH/°C meter. The analysis of aliquots collected during the photocatalytic experiments was

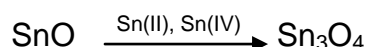
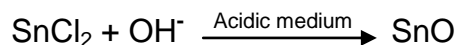
done using PerkinElmer Lambda 750 UV-Vis spectrometer. UV spectra were plotted with the help of OriginLab Corporation OriginProVer 9.0 software. Zeta potential (ξ) of SnS₂ is measured by zetasizer using a bench top Nanotracs Wave-Microtrac.

1.3 Results and Discussion:

Excess hydrazine hydrate leads to change in oxidation state of copper from Cu(II) to Cu(I). The copper hydroxide after undergoing the change of oxidation state turns in to cuprous oxide. The reactions can be expressed as:



Trisodium citrate acts a surfactant as well as capping agent and also plays a role in maintain pH of the solution. In acidic medium the oxidation state of tin changes from Sn(II) to Sn(IV). But, both of them exist creating a mixed –valance compound. TSC also prevents growth of the particles and can modify the surface of Sn₃O₄.



The nanostructures of Sn₃O₄ & Cu₂O had been investigated individually from powder XRD patterns of as-synthesized materials, presented in Figure 4 & 5. Figure 4 depicts the XRD pattern of Sn₃O₄ nanoplates, with diffraction peaks indexed to tin oxide (JCPDS 16-0737). The diffractogram shows d-values at 3.69Å, 3.29Å, 2.81Å, 2.71Å, 2.42Å, 2.23Å, 1.82Å, 1.73Å, 1.64Å, 1.52Å, 1.46Å and 1.42Å assigned to the planes (101), (111), (-210), (130), (102), (-301), (311), (2-41), (042), (312) and (0-33) respectively of the nanostructured triclinic phased Sn₃O₄.

Figure 5 matches the diffraction peak positions of cuprous oxide (JCPDS 78-2076) exactly. The diffractogram in the figure indicates the d-values 3.01Å, 2.46Å, 2.13Å, 1.74Å and 1.5Å assigned to the planes (110), (111), (200), (211) and (220) of the standard cuprite Cu₂O.

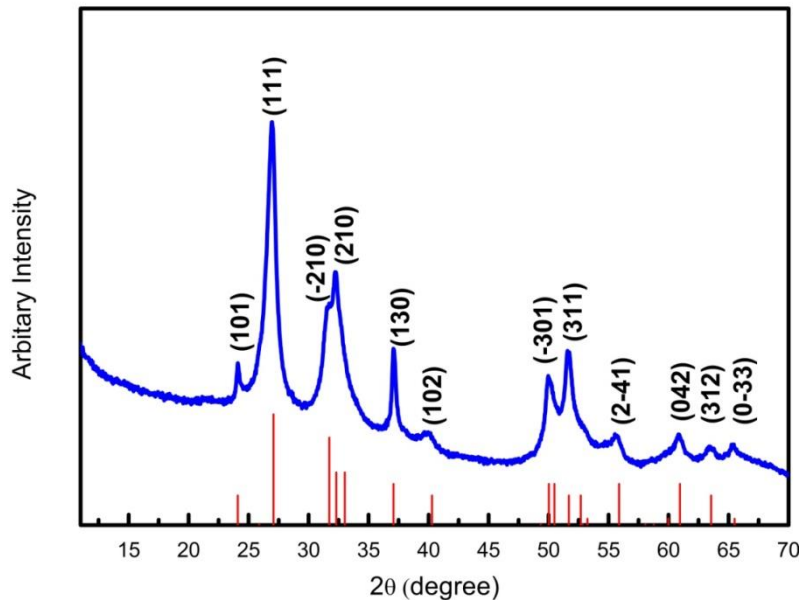


Figure 4: Powder XRD diffractogram of Sn₃O₄

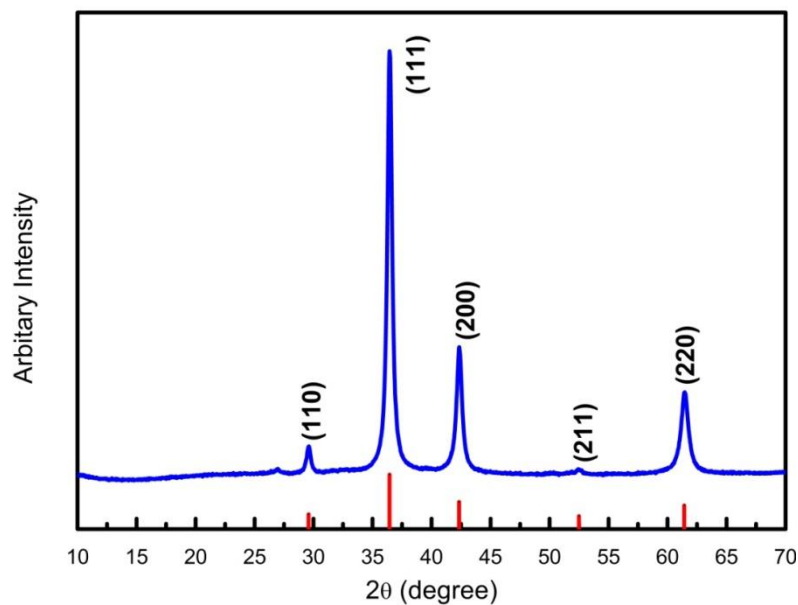


Figure 5: Powder XRD diffractogram of Cu₂O

The diffractograms of the as-synthesized heterostructures of Sn₃O₄/Cu₂O are presented in Figure 6. It can be noticed that all the diffraction peaks can be indexed characterized XRD peaks of Sn₃O₄ or Cu₂O. Those peaks matching red lines in the bottom of the graph are indexed to nanostructured Sn₃O₄ (JCPDS 16-0737) and those matching with

green lines are indexed to cuprite Cu_2O (JCPDS 78-2076). Increase in the concentration of copper can be noticed in the diffractogram, peaks marked with “*” are peaks of Cu_2O . No other peaks were observed indicating no impurities in the sample. The change in concentration of Cu_2O can also be observed with the change in the peak intensities.

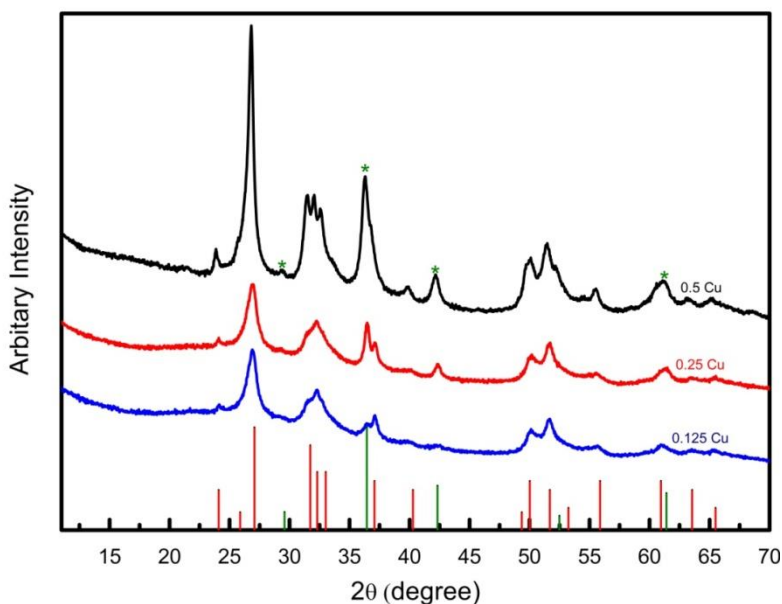


Figure 6 Powder XRD diffractogram of $\text{Sn}_3\text{O}_4/\text{Cu}_2\text{O}$ at different concentrations

The physical properties of the materials like size and shape can be observed using SEM. SEM images are of the precursors Sn_3O_4 & Cu_2O are illustrated in Figure 7, The Sn_3O_4 nanostructure shaped in the form of plates at a scale of $2\mu\text{m}$ can be observed in Figure 7a, these nanoplates are assembled together to form a hierarchical network. At a lower magnification unique flower like structure can be observed in Figure 7b. Figure 7c represents the spherical nanoparticles of Cu_2O at a scale of $1\mu\text{m}$. It can be noticed that these spherical balls are at a size of 200nm .

The morphology of the as-synthesized $\text{Sn}_3\text{O}_4/\text{Cu}_2\text{O}$ heterostructure can be seen in Figure 8. In Figure 8a, the epitaxial growth of Cu_2O on Sn_3O_4 nanoplates can be noticed. EDS helped in proving the phase purity of the sample by analysing the elemental composition of the materials. From the figure 8b it can be interpreted that the

composition of the as-synthesized materials include only oxygen, copper and tin with colours green, blue and red as labeled respectively.

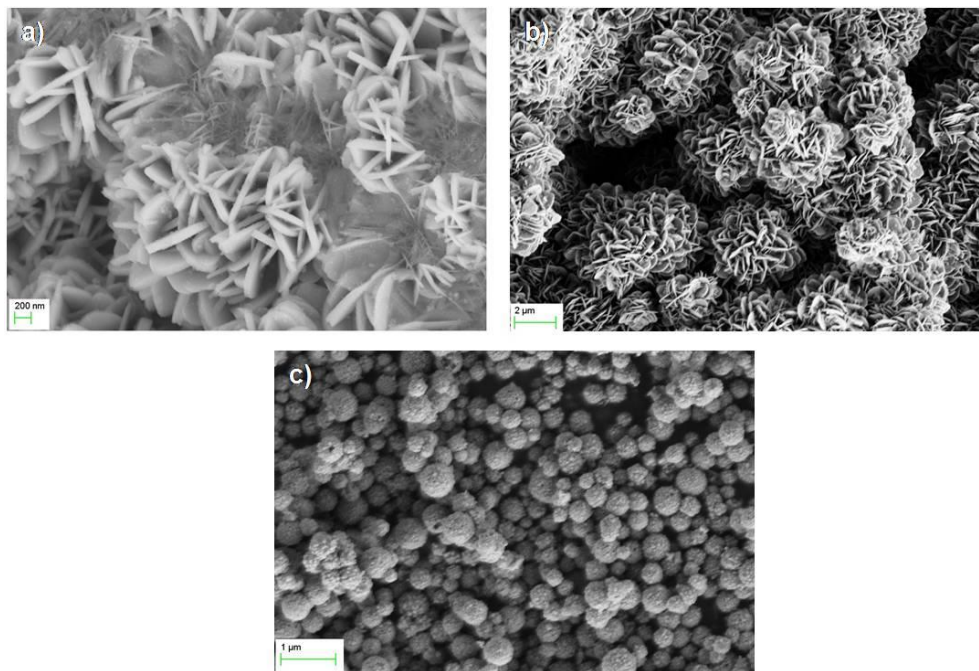


Figure 7: SEM images a) Sn_3O_4 nanoplates b) Sn_3O_4 flower like structure c) Cu_2O nanoparticles

The composition of the materials including the precursors Sn_3O_4 , Cu_2O and the heterostructure $\text{Sn}_3\text{O}_4/\text{Cu}_2\text{O}$ are presented in detail in Table 1, the increase in the concentration of copper can also be identified in this table.

Table 1: Detailed elemental composition of Sn_3O_4 , Cu_2O & $\text{Sn}_3\text{O}_4/\text{Cu}_2\text{O}$ determined using Energy Dispersive Spectroscopy (EDS)

Elements	Sn_3O_4	Cu_2O	$\text{Sn}_3\text{O}_4/\text{Cu}_2\text{O}$ 0.125 g Cu	$\text{Sn}_3\text{O}_4/\text{Cu}_2\text{O}$ 0.25 g Cu	$\text{Sn}_3\text{O}_4/\text{Cu}_2\text{O}$ 0.5 g Cu
Tin (Sn)	73.30	-	92.04	84.06	67.14
Copper (Cu)	-	66.23	7.96	15.94	32.86
Oxygen (O)	26.70	33.77	-	-	-

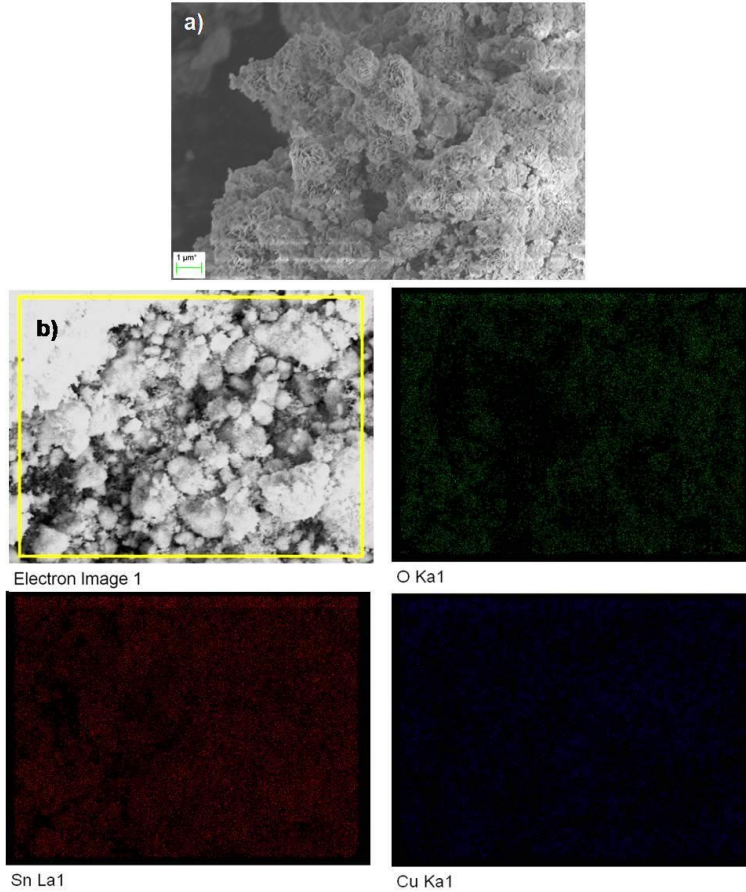


Figure 8: SEM images a) $\text{Sn}_3\text{O}_4/\text{Cu}_2\text{O}$ nanoparticles b) EDS images of heterostructure

UV-Vis diffuse reflectance spectroscopy graphs of as-synthesized precursors of Sn_3O_4 & Cu_2O are presented in Figure 9a & 9b. The steep absorption edges with respect to the colours light yellow (Sn_3O_4) and orange (Cu_2O) can be observed indicating the ability of optical absorption in the visible light region. This proves Sn_3O_4 & Cu_2O nanoparticles can be excellent materials for environmental remediation. Optical bandgap (indirect and direct) measurements of Sn_3O_4 & Cu_2O were obtained by Tauc plots [2] using the following equation:

$$(\alpha h\nu)^m = A(h\nu - E_g)$$

Where α is the absorption coefficient, $h\nu$ is incident photon energy, A is a constant relative to the material, m is an index used to characterize the optical absorption with values $\frac{1}{2}$ and 2 for indirect and direct bandgap respectively and E_g is the energy gap.

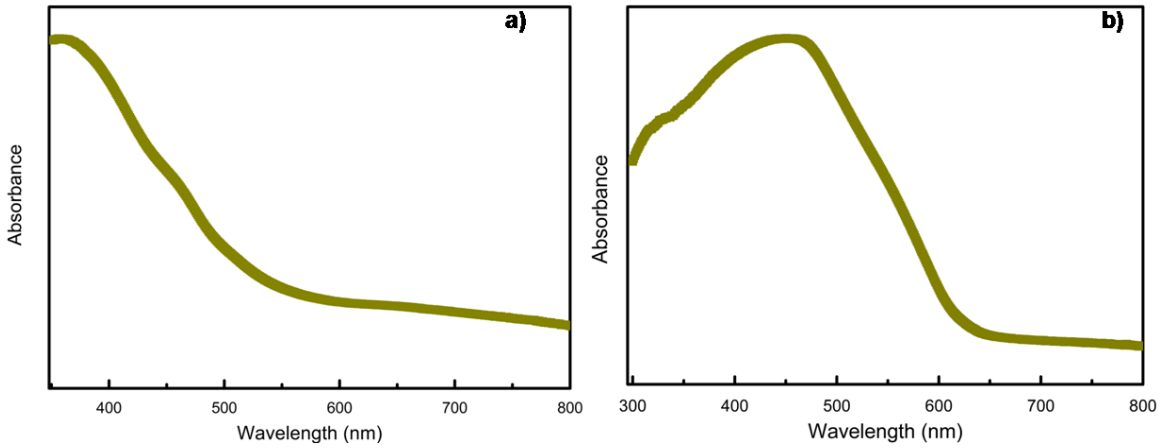


Figure 9: UV Vis diffuse reflectance spectrum a) Sn_3O_4 & b) Cu_2O

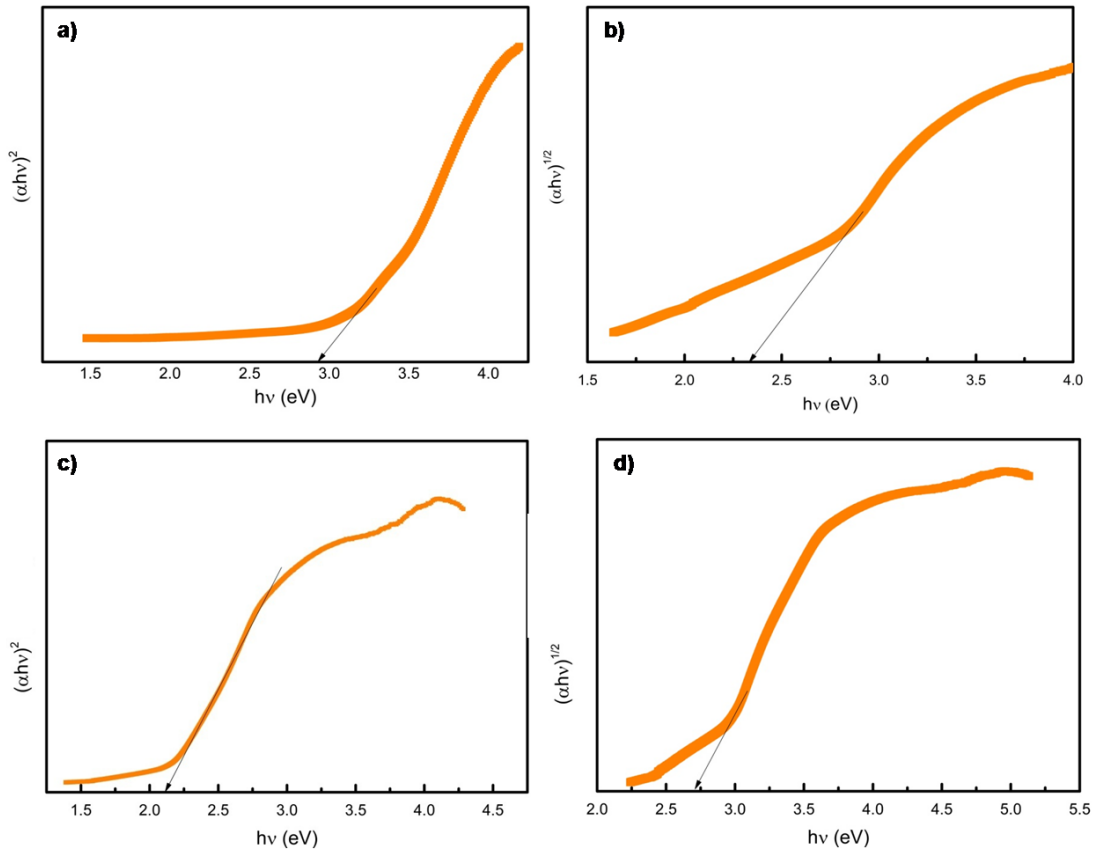


Figure 10: Plot for estimation of bandgap a) & b) direct and indirect of Sn_3O_4 c) & d) direct and indirect of Cu_2O

From the plots below in Figure 10a & 10b as-synthesized Sn_3O_4 has an indirect bandgap of 3.18eV and direct band gap of 2.92eV was observed. Hence, it is direct bandgap material with a band gap (E_g) of 2.92eV close to the bandgap reported in the

prior studies. [23] Similarly, it can be seen in Figure 10c & 10d plots of estimating the bandgap of Cu_2O nanoparticles. From the figure it can be interpreted that Cu_2O is a direct bandgap material with $E_g=2.11\text{eV}$ which is quite closer to the values reported in the literature. [25] The indirect bandgap of Cu_2O nanoparticles is 2.73eV which is higher than the direct bandgap.

UV-Vis diffuse reflectance spectroscopy graph of as-synthesized $\text{Sn}_3\text{O}_4/\text{Cu}_2\text{O}$ heterostructure with its seeding precursors is presented in Figure 11. When Cu_2O nanoparticles are grown on Sn_3O_4 nanoplates, the colour of the heterostructured photocatalyst becomes yellow and a shift in the wavelength of absorption can be seen. The redshift observed (red, pink and lines) in the heterostructure with increase in concentration is due to change in the bandgap.

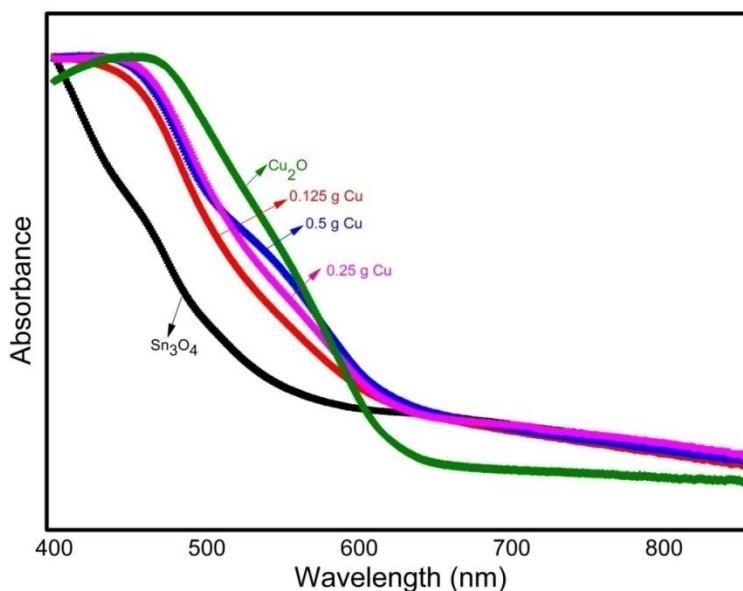


Figure 11: UV V-s diffuse reflectance spectrum of $\text{Sn}_3\text{O}_4/\text{Cu}_2\text{O}$ heterostructure

Figure 12 shows the schematic of proposed band structure of the as-prepared n-type Sn_3O_4 & p-type Cu_2O before and after fabrication of $\text{Sn}_3\text{O}_4/\text{Cu}_2\text{O}$ heterostructure.

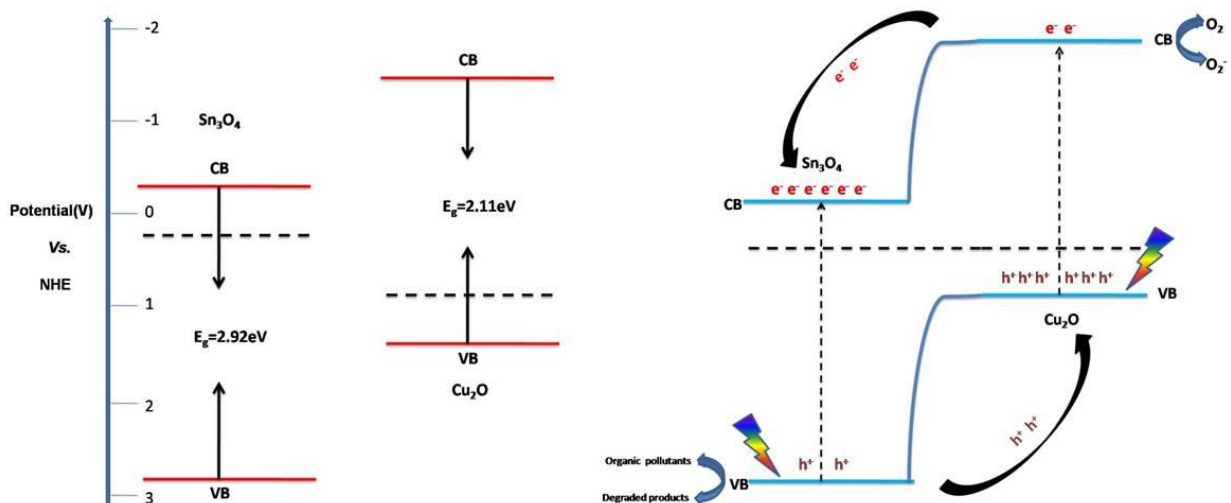


Figure 12: Schematic diagram for energy band structure of n-type Sn_3O_4 and p-type Cu_2O including the photocatalytic mechanism of fabricated $\text{Sn}_3\text{O}_4/\text{Cu}_2\text{O}$ heterostructure

Photoelectrons can be easily trapped by electron acceptors like adsorbed O_2 , NO_3^- , which serially produces a superoxide anion radical ($\bullet\text{O}_2^-$). [29] Similarly, OH^- can trap the photoinduced holes which additionally produce a hydroxyl radical species ($\bullet\text{OH}$). [30] These radicals act as a strong oxidizing agent by its attribute of accepting electrons and help in mineralization of organic pollutants. The band positions of Sn_3O_4 [31] & Cu_2O [32] was taken from the literature.

The pH dependence of zeta potential of Sn_3O_4 nanoplates in an aqueous dispersion is presented in Figure 13a. Zeta potential decreases with increase in pH following the similar patterns recorded before but, the positively charged particle always gives a positive zeta potential, even at very high pH. The concentration of the dispersion is extremely low and the measurements are done at room temperature.

The pH dependence of zeta potential of as-prepared $\text{Sn}_3\text{O}_4/\text{Cu}_2\text{O}$ heterostructure at a very low concentration in an aqueous dispersion can be observed in Figure 13b. Increase in pH led to a negative surface charge and decrease in zeta potential. But, huge variation of zeta potential was observed when changing the pH of the dispersion.

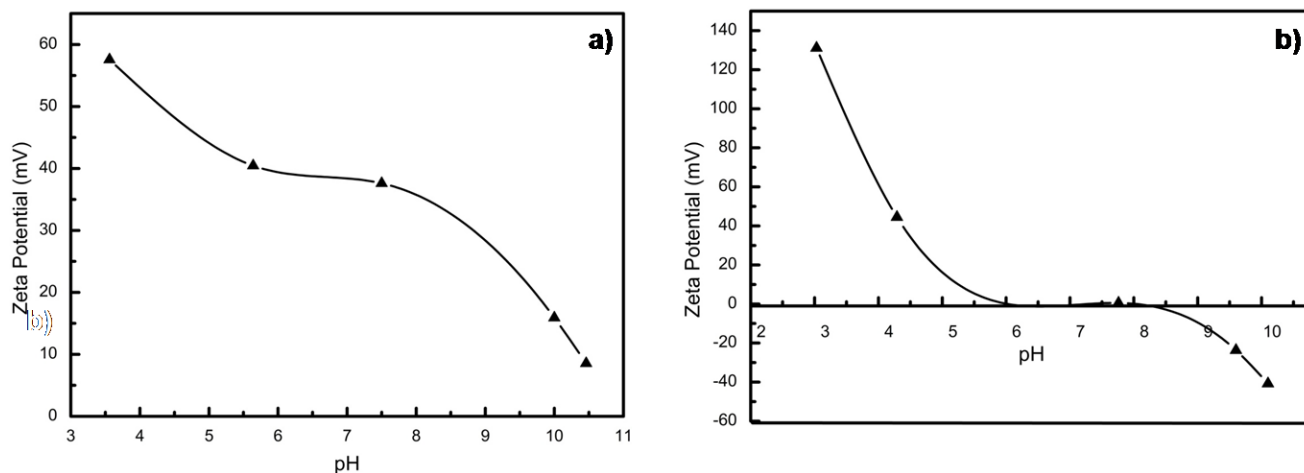


Figure 13: pH vs. Zeta potential a) Sn_3O_4 b) $\text{Sn}_3\text{O}_4/\text{Cu}_2\text{O}$ heterostructure

The photolytic activity of the catalyst was evaluated by investigating the decomposition process of the dye indigo carmine in aqueous suspension. A solution with a concentration of 1000ppm was made before each experiment and the same solution was used in whole experiment.

The IC degradation activity of the seeding precursors Sn_3O_4 nanoplates, Cu_2O nanoparticles and their $\text{Sn}_3\text{O}_4/\text{Cu}_2\text{O}$ heterostructure counter parts under visible light for 120 min can be observed in Figure 14. In spite of the fact that the degradation capabilities of $\text{Sn}_3\text{O}_4/\text{Cu}_2\text{O}$ vary at different concentrations of Cu_2O , they were all higher than the capability of the precursors Sn_3O_4 & Cu_2O . Moreover, it can be observed that the photocatalytic activity of heterostructure $\text{Sn}_3\text{O}_4/\text{Cu}_2\text{O}$ with a Cu content of 0.125 g is highest. The photocatalytic activity of $\text{Sn}_3\text{O}_4/\text{Cu}_2\text{O}$ increased with gradual decrease of Cu content, but further decrease in concentration led to decrease in the photocatalytic activity.

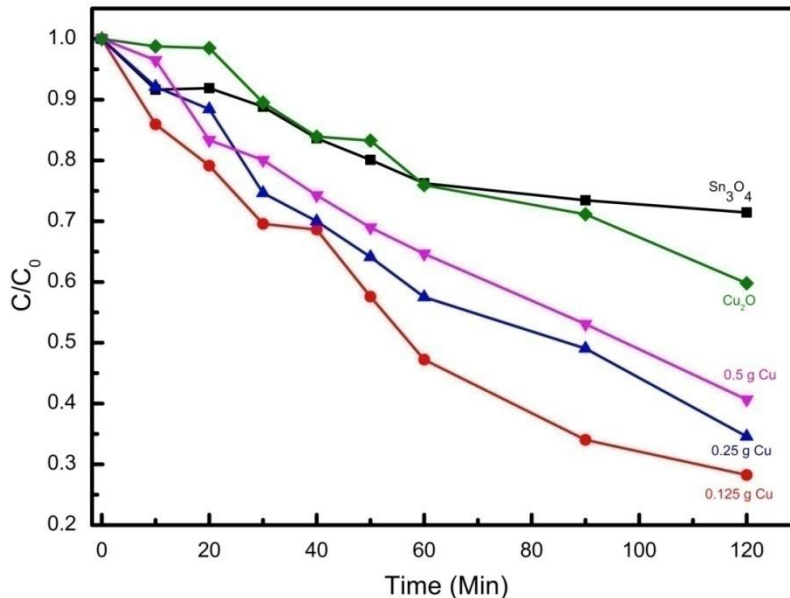


Figure 14: Degradation profile of IC by Sn₃O₄/Cu₂O at different concentrations of Cu

The catalyst with the lowest content of Cu was taken and its photocatalytic activity was evaluated at different pH. Presented in Figure 15 are the degradation profiles of Sn₃O₄/Cu₂O with Cu content 0.125 g. The initial pH of the Sn₃O₄/Cu₂O suspension was 5.69. Totally, the degradation profiles of 5 different pH solutions were investigated. The decomposition of IC of two solutions with pH below then the initial pH viz. 2.92 & 4.59 and two above viz. 8.83 & 9.91. The pH of these solutions was modified by adding 1M NaOH and HCl solutions. Noticeably, the amount organic pollutant decomposed with respect to time is more at a higher pH when compared to the other cases. Similarly, as mentioned in the previous chapter; increase in basicity above pH 11, led to change in colour of the suspension, from blue to yellow green and there were no traces of IC when recorded UV-Vis spectroscopy. In Figure 15, noticeably, the decomposition of IC was faster at a high pH viz. pH 9.91 and as the pH was decreasing the time taken for degradation increased. At pH 2.92, flocculation was observed, because Sn₃O₄/Cu₂O at pH 2 lost the stability in the medium and started to sediment.

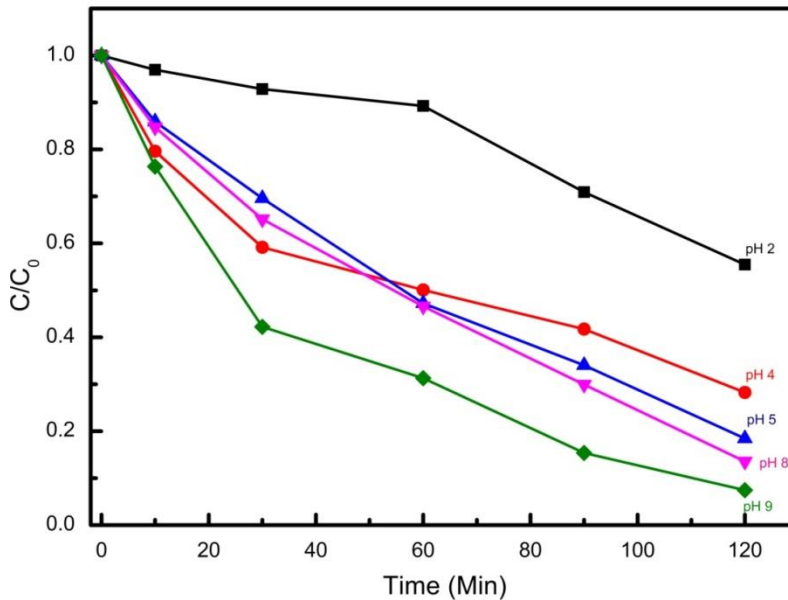


Figure 15: Degradation profile of IC by $\text{Sn}_3\text{O}_4/\text{Cu}_2\text{O}$ (0.125 g of Cu) at different pH

Figure 16 is an example of UV Vis spectrum of $\text{Sn}_3\text{O}_4/\text{Cu}_2\text{O}$ (0.125 g of Cu) at pH 9.91. It was noticed that $\text{Sn}_3\text{O}_4/\text{Cu}_2\text{O}$ is a stable photocatalyst as the powder XRD after a cycle of degradation showed the same crystallinity as the observed in as-prepared heterostructure.

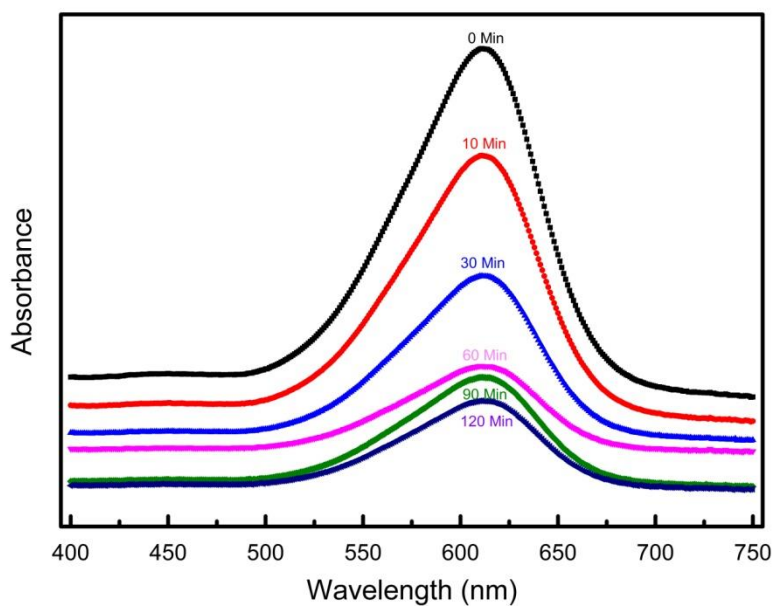
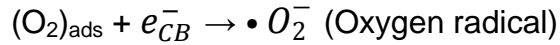
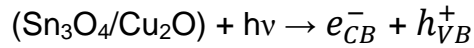
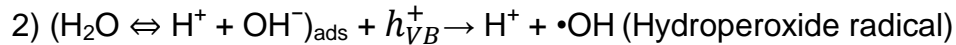
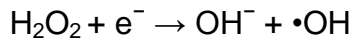
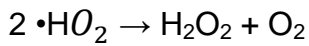
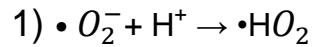


Figure 16: UV Vis spectrum of decomposition of IC by $\text{Sn}_3\text{O}_4/\text{Cu}_2\text{O}$ at pH 9.91

Among all the oxidation methods photocatalysis appears to be leading to total mineralization of organic pollutant following the proposed mechanism below: [12]

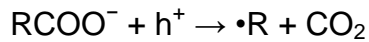


Hydroperoxide radical can be developed in two different ways:



These hydroperoxide radicals break various C-N and C-C bonds of the chromophore group present in the dye molecule leading to discolouration at first. Further it totally mineralizes into CO_2 .

Here holes can also react directly with carboxylic acids, generating carbon dioxide. This specific reaction is called photo-Kolbe reaction as reported. [11]



1.4 Conclusion:

In conclusion, we have investigated mainly about $\text{Sn}_3\text{O}_4/\text{Cu}_2\text{O}$ heterostructure and the photocatalytic activity under visible light irradiation. In particular, $\text{Sn}_3\text{O}_4/\text{Cu}_2\text{O}$ was optimized by evaluating the decomposition of Indigo carmine at different concentrations of copper. Even the pH dependent photocatalysis was investigated by changing the pH of the suspensions. However, the photocatalytic performance of these materials was tested with a 400 Watt metal halide lamp, it is expected that the degradation ability will be better than this when performed under a solar simulator (Xenon lamp). We are optimizing $\text{Sn}_3\text{O}_4/\text{Cu}_2\text{O}$ thin film for its further applications on visible light driven photocatalysis and photovoltaics.

Chapter 2:

2.1 Synthesis of SnS₂ nanoflakes and its photocatalysis

Tin being an abundant material also has most number of stable isotopes over all the other elements in the periodic table. In recent research, sulfides and oxides of tin had been extensively pursued and investigated in many applications. One of the most important and trending application in the field of physical chemistry is photocatalysis and hydrogen fuel generation through splitting water.

Tin sulfide is a low toxic material with a good stability; it is an n-type semiconductor with interesting photo conductive properties which are helpful in applications of opto-electrical devices. It is a wide band gap material 2.18 eV. [7] It has a layered structure with the properties of a hexagonal crystal system. [8]

By changing the concentration of reactants, temperature or duration of the reaction the morphology of the material can be altered. Therefore, SnS₂ has been fabricated into hierarchal nanoflaked layered structure through following a standard prescription in the literature. [9]

2.1.1 Experimental procedure:

Synthesis procedure:

SnS₂

SnS₂ was synthesized by the route of hydrothermal synthesis in a 50 mL Teflon lined stainless steel autoclave reactor. A mixture of Tin(II) chloride SnCl₂ (0.379 g, 2 mmol) and Thioacetamide C₂H₅NS (1.878 g, 25 mmol) were dissolved in 40 mL of deionized water.[9] The solution was stirred for 30 min and transferred to a Teflon vessel autoclave reactor. After heating in an electric heater at 160°C for 24 h, the reactor was cooled to room temperature. This reaction has H₂S as its by-product; hence it is advised to put the reactor under an exhaust. The colour of the obtained final product was dark yellow-brown.

All the chemicals were purchased from Sigma Aldrich and SDL, and directly used without additional purification.

Photocatalytic experiments:

Photocatalytic properties of the above synthesized SnS_2 were investigated by evaluating the degradation profiles of Indigo carmine ($\text{C}_{16}\text{H}_8\text{N}_2\text{Na}_2\text{O}_8\text{S}_2$) using a metal halide lamp. The photocatalysis experiments were implemented using an apparatus set up in our lab, including four parts: a metal halide lamp, cooling attachment preventing overheating of the lamp by circulating cold water and magnetic stirrer. All the experiments were performed in 30 mL glass vials at room temperature. These glass vials were placed at a distance of 10 cm away from the lamp. Before irradiating; 10 mg of IC was dissolved in 10 mL of DI water to make a 1000 ppm solution and stored in a dark place. 20 mg of the active material was taken in 19 mL of DI water and an aliquot of 1 mL IC was added. Subsequently, the solution was magnetically stirred in dark for 2 h for the photocatalyst and the dye to attain adsorption/desorption equilibrium. During irradiation, 1 mL aliquots were collected from the reaction cell using a micro pipette at a 10 min interval for 60 min. The collected suspensions were subjected to centrifugation in order to separate the active material. Centrifugation was performed at high rpm (10000 rpm).

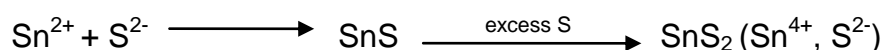
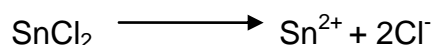
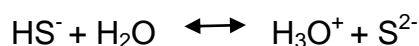
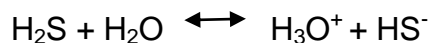
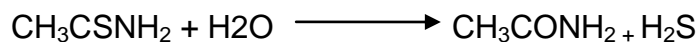
The degradation profiles of the active material were investigated at different pH. Initial pH of the solution was 4.53 and was altered using 1M aqueous solutions of NaOH and HCl. Different pH of solutions were as follows 2.86, 3.47, 4.93, 7.49, 9.98. pH of the solution was altered before adding the dye.

2.1.2 Results and discussion:

Reactions process of formation of SnS_2 is as follows:

In the course of reaction, thioacetamide hydrolyzes and tends to release S^{2-} gradually. The control of nucleation of SnS_2 depends on the rate at which S^{2-} is released. Specific parameters like temperature, duration of the reaction and concentration of the reactants

which influence the nucleation and hydrolysis rate of TAA had been optimized carefully for desired properties and morphology. [1]



Hence, to increase the yield, the duration of time was increased to 24 h rather than 12 h as prescribed in the literature followed. Initially due to this, SnS was formed and as there was a gradual increase in the amount of sulphur, tin was oxidized from Sn^{2+} to Sn^{4+} and formation of SnS_2 was observed.

Powder X-ray diffraction (XRD) pattern of the final product is presented in Figure 17 where all the peaks are indexed to berndtite SnS_2 from Joint Committee on Powder Diffraction Standards (JCPDS 23-0677). The XRD pattern has the d-values of 5.89Å ; 3.162Å ; 2.784Å ; 2.155Å ; 1.824Å ; 1.743Å ; 1.669Å and 1.526Å assigned to the planes (001), (100), (101), (102), (110), (111), (103) and (201) respectively. Lack of extra peaks in the pXRD pattern explains the absence of by-products and the purity of the sample.

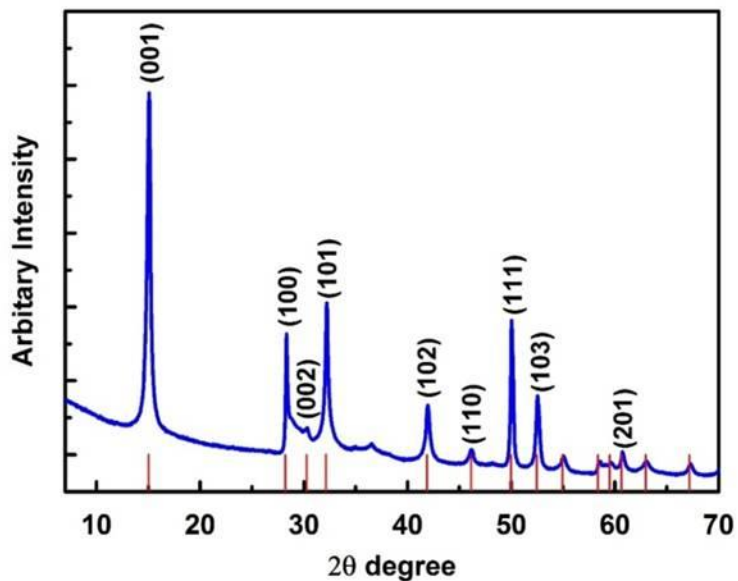


Figure 17: Powder XRD diffractogram of SnS₂ nanoflakes

Morphological investigation of SnS₂ was performed using SEM images. SEM images are illustrated in Figure 18. The shape and size of SnS₂ nanoflakes are observed in Figure 18b. These nanoflakes assembled together to form a hierarchical networks presented in Figure 18a.

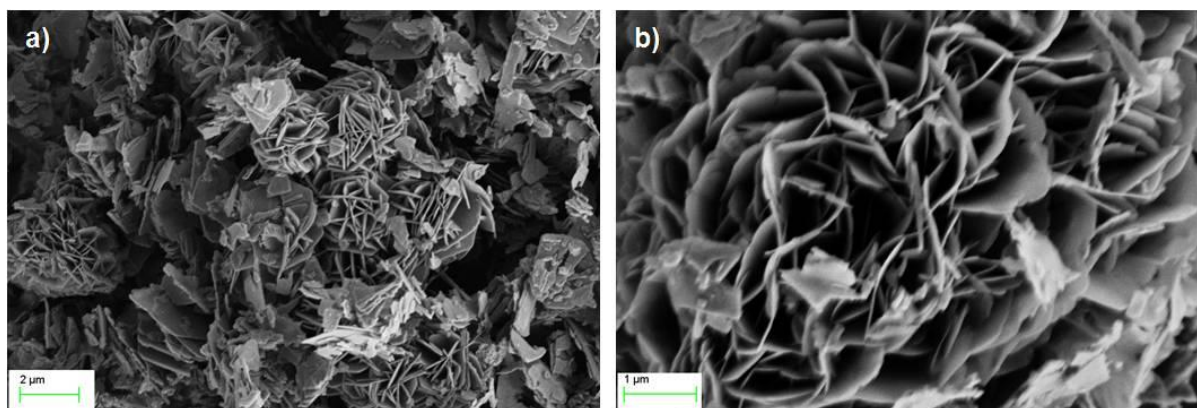


Figure 18: SEM images of SnS₂ a) hierarchical network b) SnS₂ nanoflakes

UV-Vis diffuse reflectance spectroscopy of as-synthesized SnS₂ is presented in Figure 19. From the figure it can be interpreted that the material has the capability of optical

absorption in the visible light region. This proves SnS₂ nanoflakes tend to be an excellent candidate for environmental remediation. Optical bandgap (indirect and direct) measurements of SnS₂ were obtained by Tauc plots [2] using the following equation:

$$(\alpha h\nu)^m = A(h\nu - E_g)$$

Where α is the absorption coefficient, $h\nu$ is incident photon energy, A is a constant relative to the material, m is an index used to characterize the optical absorption with values $\frac{1}{2}$ and 2 for indirect and direct bandgap respectively and E_g is the energy gap.

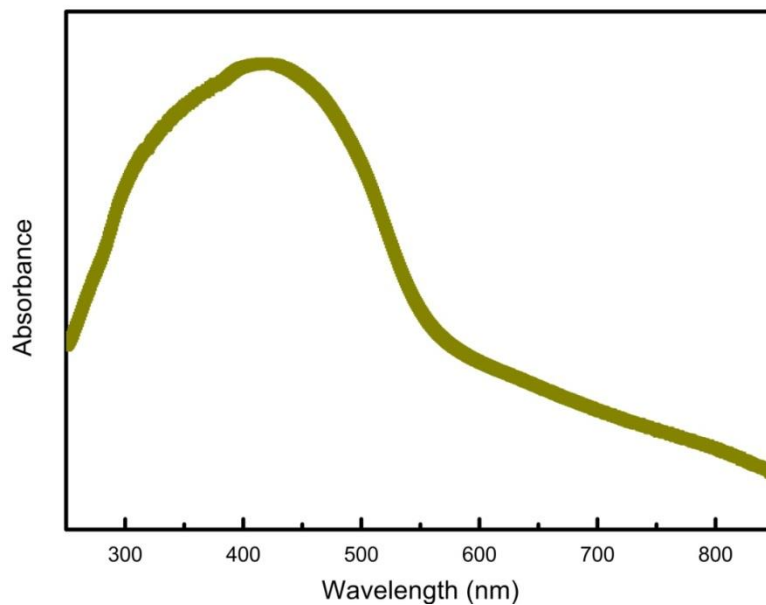


Figure 19: Diffuse reflectance spectra of SnS₂

The curve of $(\alpha h\nu)^2$ versus $h\nu$ is presented in Figure 20. The bandgap of the material is calculated by extending the linear part in the curve till it touches the x-axis and the point at which the extension touches the x-axis is considered as the bandgap of the material. The direct bandgap of SnS₂ nanoflakes is less than indirect bandgap, hence it is considered as a direct bandgap material. Bandgap observed in this case was 2.18 which were very near to the reported value.

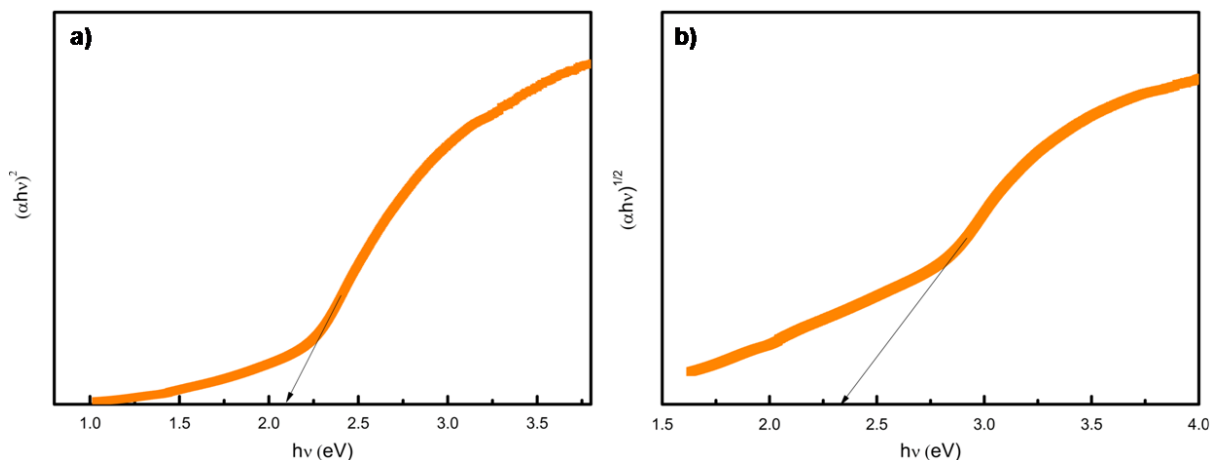


Figure 20: Plot for estimating the bandgap of SnS₂ a) direct bandgap $(\alpha h\nu)^{1/2}$ vs. $h\nu$ b) indirect bandgap $(\alpha h\nu)^2$ vs. $h\nu$

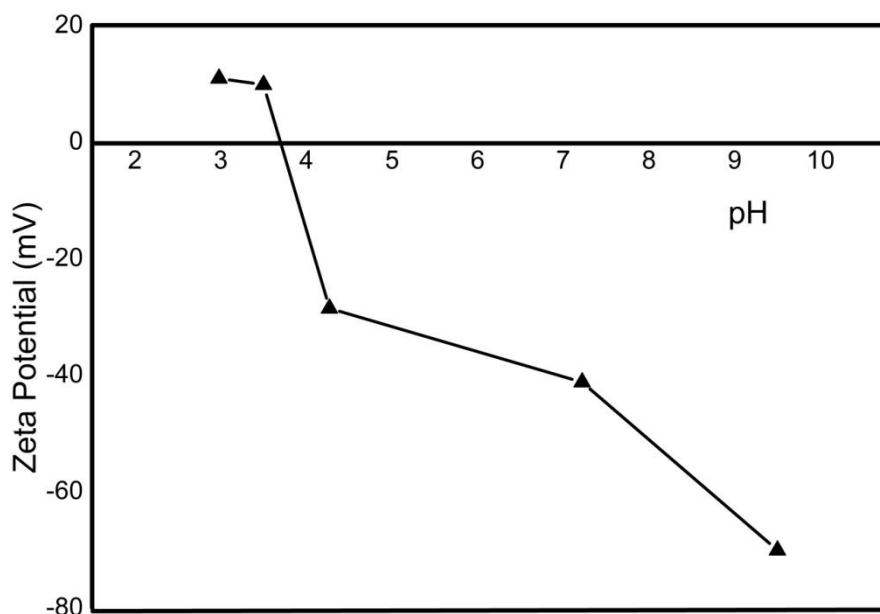


Figure 21: pH vs. Zeta potential of SnS₂

The pH dependence of zeta potential of SnS₂ nanoflakes in an aqueous dispersion is presented in Figure 21. In this dispersion of very low concentration the zeta potential of nanoflakes decreased with increase in pH. The SnS₂ nanoparticles are positively charged exhibiting a positive zeta potential in acidic pH. Conversely, a negatively

charged zeta potential was observed in basic medium. These results are quite closer to the results observed in literature. [10]

The photocatalytic degradation profiles of the catalysts were investigated by monitoring the decomposition process of the dye indigo carmine in aqueous suspension. A solution with a concentration of 1000ppm was made before each experiment and the same solution was used in whole experiment.

In these experiments commercially available Degussa p-25 TiO_2 was used as a reference to study the photocatalytic activity of the as-synthesized SnS_2 . The photocatalytic activities of SnS_2 at different pH are evaluated and are presented in the Figure 22. Initial pH of SnS_2 suspension was 4.93. Hence the pH of the solution was altered into 4 different cases, two solutions at pH below the initial pH viz. 2.86 & 3.47 and two above viz. 7.49 & 9.98. The pH of these solutions was modified by adding 1M NaOH and HCl solutions. As in the figure, on y-axis C_0 is the initial concentration of equilibrium adsorption of IC and C is the initial reaction concentration of IC. X-axis is labeled with time taken for the degradation of dye in minutes. As seen in the figure, the degradation of IC is negligible and SnS_2 nanoflakes exhibit higher photocatalytic activity compared to Degussa p-25. In this case, in 60 min of time total discolouration of IC is noticed in all SnS_2 solutions compared to Degussa p-25. The highest photocatalytic activity can be observed in the solutions with a lower pH. As IC is an anionic dye, it is more adsorbed and degraded at a lower pH. This is due to the electrostatic interaction between the dye and catalyst surface. Basing on this observation, it can be said that the degradation of an organic pollutant also depends up on the pH of the solution. Decomposition of the substrate is possible at a higher pH but at a lower rate comparatively.

Figure 23 is an example of how a UV Vis spectrum looks like, it represents the photocatalytic activity of SnS_2 at pH 4.93. In addition, SnS_2 has an excellent catalytic stability; because after a full degradation cycle, the catalyst from the remaining solution is centrifuged out by washing it several times with distilled water and ethanol. Then the collected sample was subjected to drying at 60°C under vacuum. A powder XRD

pattern of the acquired catalyst was recorded and same crystallinity of the synthesized sample was observed.

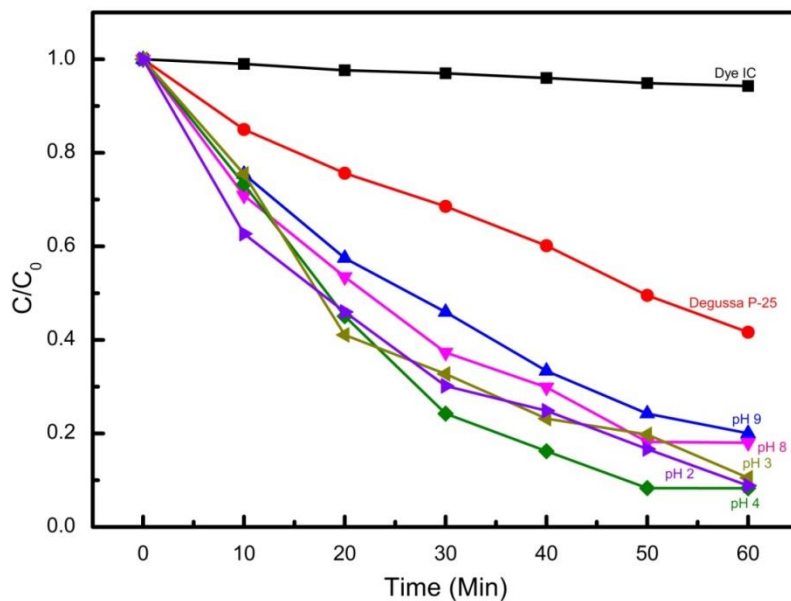


Figure 22: Degradation profiles of IC by SnS₂ at various pH

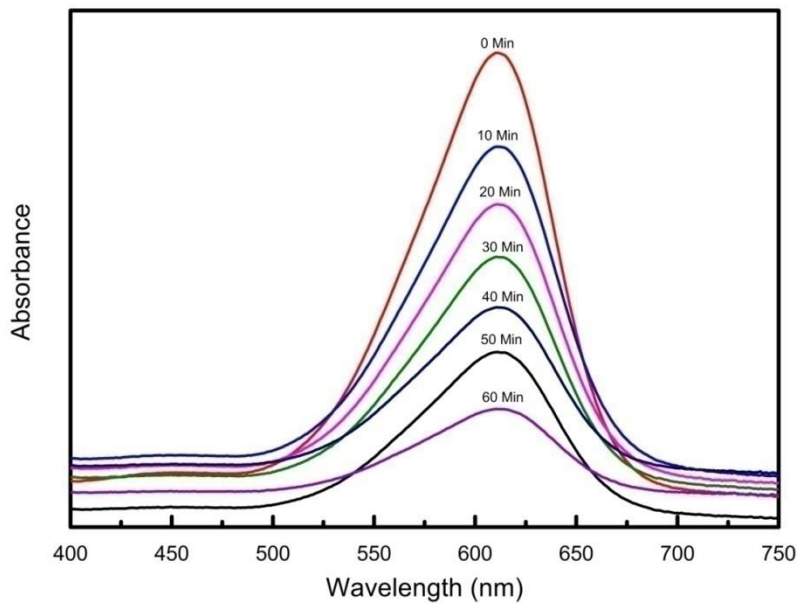


Figure 23: UV Vis spectrum of decomposition of IC by SnS₂ at pH 4.93

2.2 SnS₂/KNbO₃ heterostructure for enhanced photocatalytic activity

Semiconductor assemblies are extensively used in photocatalysis, generating hydrogen fuels, solar cell etc. Using two different semiconductors with different band energies and their band positions has been considered one of the better ways to enhance the visible-light driven photocatalysis. Hence, semiconductors with different redox energies were chosen and novel heterostructures were synthesized to enhance the ability of photocatalysis.

Nano sized metal oxides, especially Nickel (II) oxide NiO was extensively studied due to its magnetic properties [13] and applications in electrochemical capacitors, photochemical solar cells. [14] Mainly, NiO was chosen as it is a p-type semiconductor with wide band gap, capable of forming n-p hetero-junction with SnS₂.

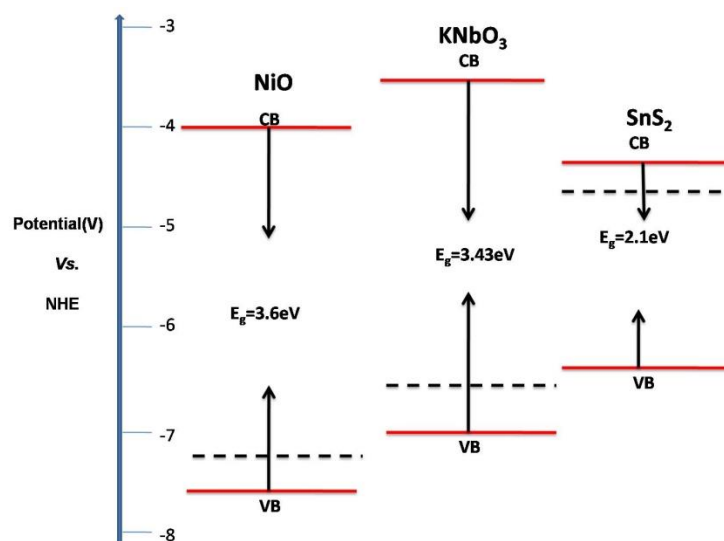


Figure 24: Proposed band configuration of NiO, KNbO₃, SnS₂

A proposed band configuration of NiO, KNbO₃, and SnS₂ is presented in Figure 24. From the figure it can be interpreted that NiO & KNbO₃ are p-type [20, 37] semiconductors capable of forming a heterostructure with n-type SnS₂. The band positions of NiO [20], KNbO₃ & SnS₂ [36] are taken from literature. But, NiO when fabricated into a heterostructure was having an impurity of NiS. Hence, KNbO₃ was chosen and been fabricated into a heterostructure without any impurities.

Perovskite materials (ABO_3) had been identified as low-priced foundation for highly productive photovoltaics [16] and many other applications viz. environmental remediation and clean energy production etc. [15]. Potassium niobate $KNbO_3$ being a ferroelectric nanomaterials with perovskite structure showed some effective results when fabricated into heterostructure with SnS_2 .

Therefore, a standardized heterostructure was fabricated and an investigation observing the degradation profiles of individual $KNbO_3$ followed by its heterostructures were performed.

2.2.1 Experimental procedure:

Synthesis procedure:

NiO:

NiO nano-particles were synthesized using hydrothermal method followed by calcinations at 500°C over different periods of time. Size of NiO was smaller compared to the size of SnS_2 . As-synthesized materials were taken and subjected to fabrication under hydrothermal conditions to make a heterostructure with SnS_2 . The growth kinetics was elucidated and it was found that the desired heterostructures were not formed. Instead, the oxygen in NiO had been replaced by the excess sulphur during the course of the reaction.

$KNbO_3$:

$KNbO_3$ was synthesized by hydrothermal route [17] in a 40 mL Teflon lined stainless steel autoclave reactor. Potassium hydroxide KOH (16.8 g, 10 M) and Niobium Sesquioxide Nb_2O_3 (0.53 g) were taken in 30 mL DI water and subjected to vigorous stirring for 15 min. The solution was transferred to a Teflon lined reactor and heated to 200°C for 5 h. After cooling the autoclave to room temperature, a yellowish solid precipitate was observed. The obtained precipitated was separated by centrifugation and washed it several times with distilled water and ethanol. The product obtained was then dried at 60°C under vacuum.

Heterostructure SnS₂/KNbO₃:

The heterostructure of SnS₂ and KNbO₃ was fabricated through the route of hydrothermal synthesis. Above synthesized Potassium Niobate KNbO₃ (0.150 g) was taken in 30 mL of DI water and stirred for 10 min, followed by the addition of Tin(IV) chloride SnCl₄ (0.26 g, 1 mmol) and Thioacetamide C₂H₅NS (0.15 g, 2mmol). The stirring was continued for 30 more min. The solution was then transferred to 40 mL Teflon tank reactor which was heated at 150°C for 12 h. After cooling the autoclave to room temperature, the obtained precipitate was subjected to centrifugation by washing it several times with distilled water and ethanol. Then the collected product was dried at 70°C in a vacuum oven. The colour of the obtained product was yellow.

All the chemicals were directly purchased from Sigma Aldrich and SDL, and used without additional purification.

Photocatalytic experiments:

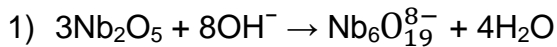
Firstly, photocatalytic properties of the above synthesized precursors *viz.* SnS₂ & KNbO₃ were investigated by evaluating the degradation profiles of Indigo carmine (C₁₆H₈N₂Na₂O₈S₂) using a metal halide lamp.

The photocatalysis experiments were implemented using an apparatus set up in our lab, including three parts: a metal halide lamp, cooling attachment preventing overheating of the lamp by circulating cold water and a magnetic stirrer. All the experiments were performed in cylindrically shaped 30 mL glass vials, at room temperature. These glass vials were placed at a distance of 10 cm away from the lamp. Before irradiating; 10 mg of IC was dissolved in 10 mL of DI water to make a 1000 ppm solution and stored in a dark place. 20 mg of the active material was taken in 19 mL of DI water and an aliquot of 1 mL IC was added. Subsequently, the solution was magnetically stirred in dark for 2 h for the photocatalyst and the dye to attain adsorption/desorption equilibrium. During irradiation, 1 mL aliquots were collected from the reaction cell using a micro pipette at a 10 min interval for 60 min. The collected suspensions were subjected to centrifugation in order to separate the active material. Centrifugation was performed at high rpm (10000 rpm).

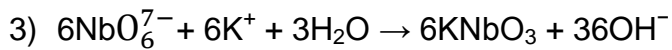
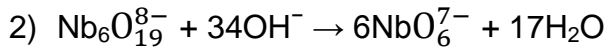
The degradation profiles of the $\text{SnS}_2\text{-KNbO}_3$ heterostructures were investigated at different pH. Initial pH of the solution was 7.22 and was altered using 1M aqueous solutions of NaOH and HCl. Different pHs of solutions are as follows 4.5 and 9.87. pH of the solution was altered before adding the dye.

2.2.2 Results and Discussion:

The reaction of the precursor KNbO_3 can be expressed as:



Formation of monomer from hexaniobate ion:



The generated monomer reacts with potassium ion to form the required perovskite structure. [17] Specific parameters like temperature, duration of the reaction and concentration of the reactants which influence the control of nucleation are optimized carefully for desired properties and morphology. [18]

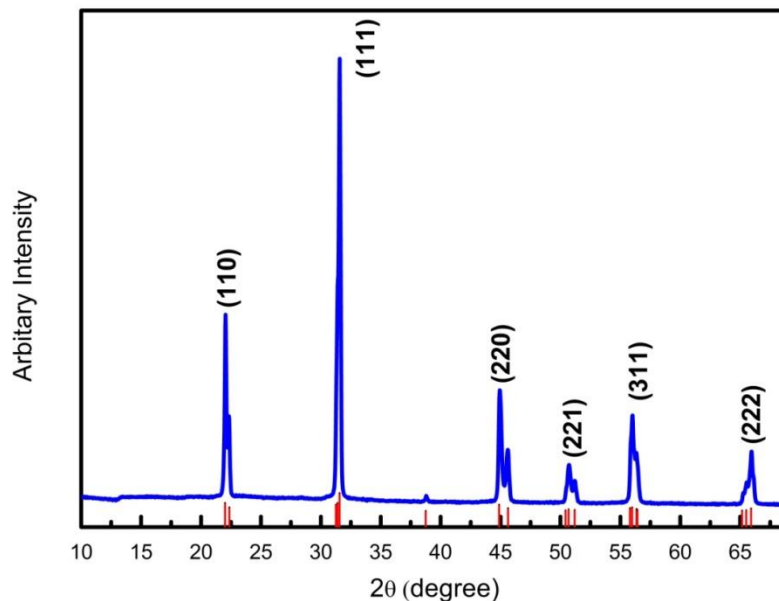


Figure 25: Powder XRD diffractogram of the perovskite structure KNbO_3

Figure 25 shows the powder XRD patterns KNbO_3 . KNbO_3 can be indexed to orthorhombic phase of potassium niobium oxide (JCPDS 32-0822). The diffractogram of KNbO_3 has the d-values 4.035\AA , 2.832\AA , 2.018\AA , 1.79\AA , 1.64\AA and 1.416\AA , assigned to the planes (110), (111), (220), (221), (311) and (222) respectively. Lack of extra peaks in the pXRD pattern explains the absence of by-products and the purity of the sample.

The diffractogram of the as-synthesized heterostructures of $\text{SnS}_2/\text{KNbO}_3$ is presented in Figure 26. It can be noticed that all the diffraction peaks can be indexed characterized XRD peaks of SnS_2 or KNbO_3 . Those peaks marked with 'colour green' are indexed to berndtite SnS_2 (JCPDS 23-0677) and those with 'colour red' are indexed to orthorhombic KNbO_3 (JCPDS 32-0822). No other peaks were observed indicating no impurities in the sample.

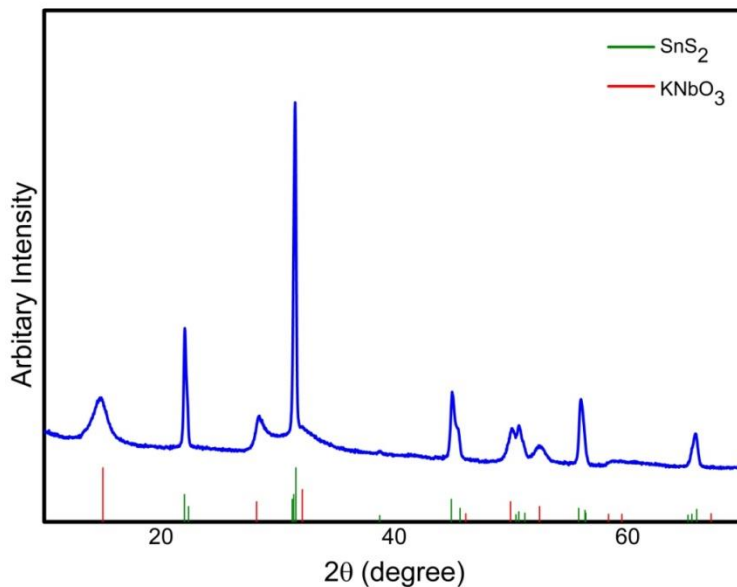


Figure 26: Powder XRD diffractogram of the heterostructure $\text{SnS}_2/\text{KNbO}_3$

Morphological investigation of as-prepared KNbO_3 and $\text{SnS}_2/\text{KNbO}_3$ was performed using SEM images illustrated in Figure 27 & 28. Figure 27a represents irregularly shaped micro particles of KNbO_3 at a scale of $2\mu\text{m}$, whereas; Figure 27b represents the

energy dispersive spectroscopy (EDS) image focused at a particular area. The elemental composition of the material can be observed from Table 2.

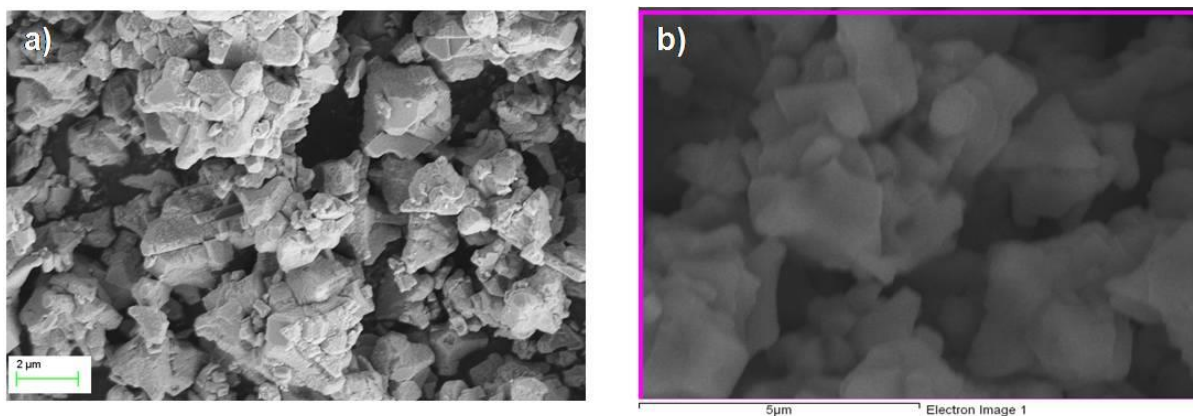


Figure 27: SEM images of KNbO₃ a) FE-SEM image b) EDS Image focused at a particular area

SnS₂ nanoflakes changed their preferential growth pattern on the varied KNbO₃ which has different crystallographic surface. This is driven due to the decrease in the distortion energy generated by lattice mismatch at both the interfaces. [22] When SnS₂ was grown on KNbO₃, the amount of tin con content dominates the surface KNbO₃. Figure 28a represents the energy dispersive spectroscopy (EDS) image focused at a particular area. The elemental composition of the heterostructure was determined using EDS and presented in Table 2. In Figure 28b colour red shows the amount of oxygen present in the focused area, similarly, green resembles potassium, white resembles tin, blue resembles niobium and purple resembles the amount of sulphur.

Table 2: Detailed elemental composition of KNbO₃ & SnS₂/ KNbO₃ determined using Energy Dispersive Spectroscopy (EDS)

Elements	KNbO ₃	SnS ₂ /KNbO ₃
Potassium (K)	18.14	5.59
Tin (Sn)	-	40.08
Sulphur (S)	-	21.31
Oxygen (O)	25.76	15.02
Niobium (Nb)	56.1	18.00

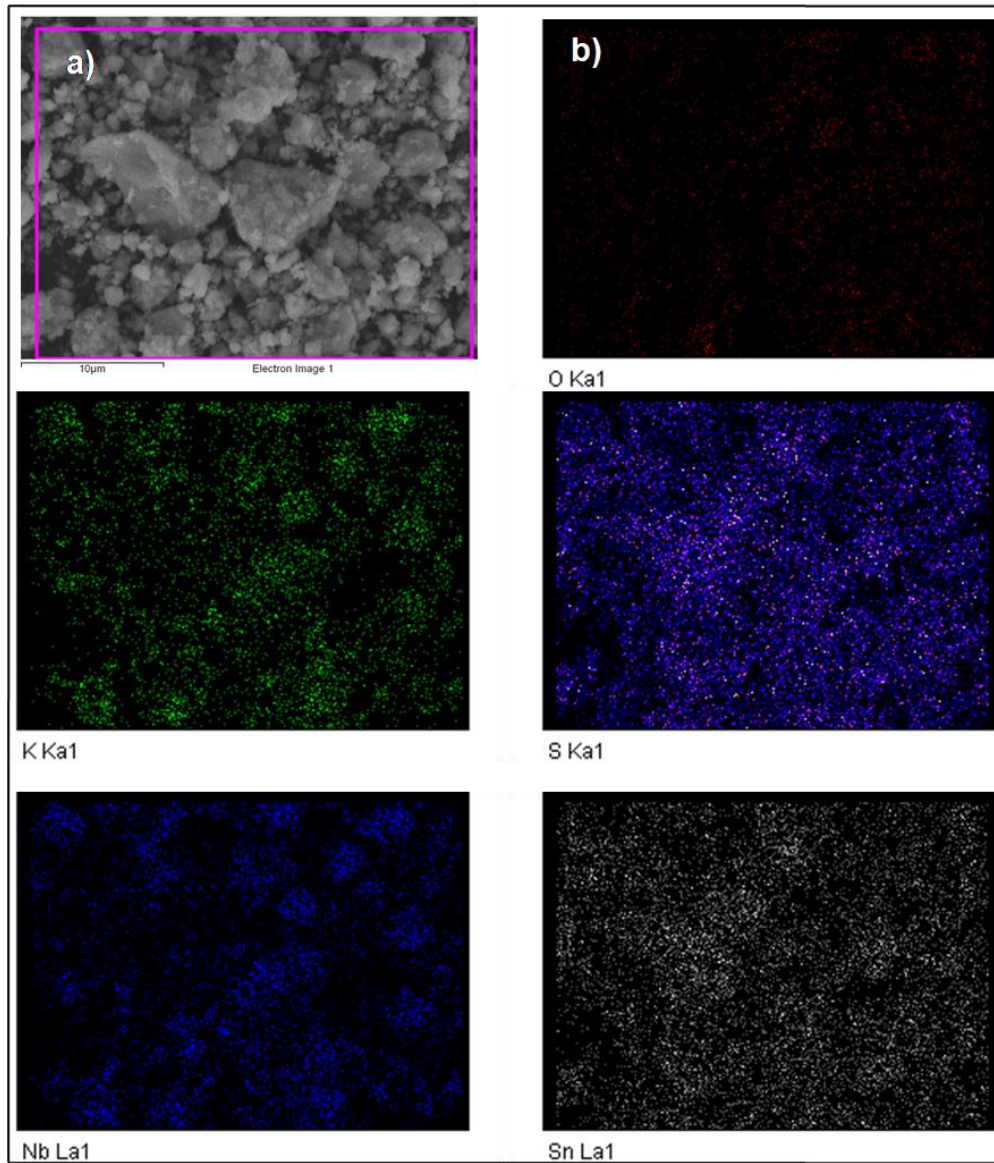


Figure 28: SEM images of $\text{SnS}_2/\text{KNbO}_3$ a) EDS image focused at a particular area b) element wise composition in the heterostructure SnS_2/KNbO

UV-Vis diffuse reflectance spectroscopy of as-synthesized KNbO_3 is presented in Figure 29. A steep absorption edge can be noticed at 300nm resembling its colour white. This spectrum determines the absorption properties of the material. [19] From the figure it can be interpreted that the material has a less capability towards optical absorption in

the visible light region. This proves the perovskite structured KNbO_3 can be a candidate for environmental remediation.

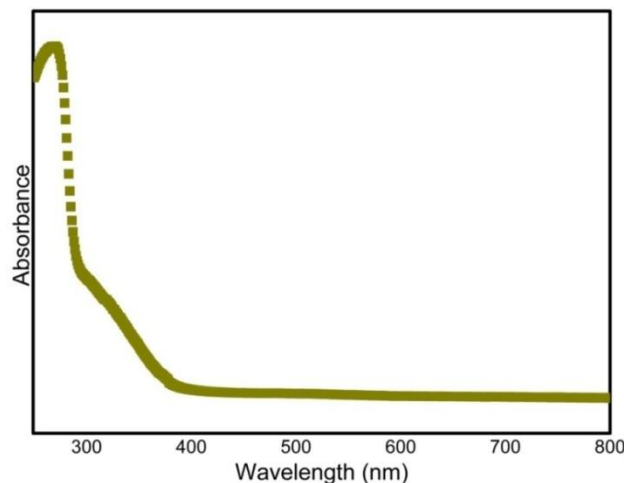


Figure 29: UV-Vis diffuse reflectance spectra of KNbO_3

In Figure 30 the UV Vis diffuse reflectance spectroscopy of the heterostructure $\text{SnS}_2/\text{KNbO}_3$ including its precursors can be observed. It is noticed that as-prepared $\text{SnS}_2/\text{KNbO}_3$ has absorption capabilities in the visible light region at a wavelength range of 400-700nm. This observation suggests, it can be an efficient material for organic dye degradation.

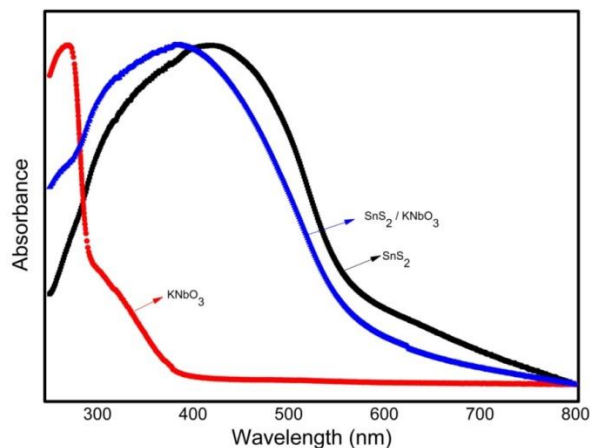


Figure 30: UV Vis diffuse reflectance spectra of $\text{SnS}_2/\text{KNbO}_3$ comparing with its precursors

When SnS₂ nanoflakes are grown on KNbO₃ microparticles the colour of SnS₂/KNbO₃ heterostructure changed to yellow explaining a redshift in the figure 30.

When SnS₂ nanoflakes are grown on KNbO₃ nanoparticles the pH dependence of zeta potential of SnS₂/KNbO₃ follows the pattern similar to the precursor SnS₂ because the surface is flooded with SnS₂. This can be observed in Figure 31. Increase in pH led to decrease in zeta potential of the heterostructure. This experiment was done in an aqueous dispersion at a very low concentration of 20mg in 200 mL of distilled water.

The charge of the particle was positive and exhibiting a positive zeta potential at pH < 5. Negatively charged zeta potential was observed in SnS₂/KNbO₃ at alkaline pH. At a lower pH the as-synthesized heterostructure has a positive charge making it an excellent photocatalyst for an anionic dye.

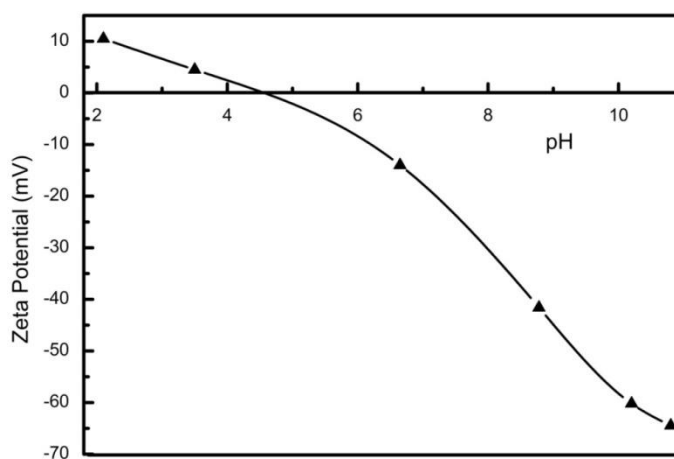


Figure 31: pH vs. Zeta potential of heterostructure SnS₂/KNbO₃

The photolytic activity of the catalyst was evaluated by investigating the decomposition process of the dye IC in aqueous suspension. A solution with a concentration of 1000ppm was made before each experiment and the same solution was used in whole experiment.

The IC degradation activity of the seeding precursors SnS₂ at its initial pH, KNbO₃ nanoparticles and their SnS₂/KNbO₃ heterostructure counter parts under visible light for

60 min can be observed in Figure 32. In spite of the fact that the degradation capabilities of $\text{SnS}_2/\text{KNbO}_3$ vary at different pH, they were all higher than the capability of the precursor KNbO_3 . With increase in acidity level, the degradation capability of the heterostructure $\text{SnS}_2/\text{KNbO}_3$ increased. Conversely, increase in pH led to a slower rate of degradation. Further increase in basicity

led to change in colour of the suspension, from blue to yellow green and there were no traces of IC when recorded UV-Vis spectroscopy. The initial pH of the $\text{SnS}_2/\text{KNbO}_3$ suspension was 7.22. Two solutions with different pH were taken, pH < In pH viz. 4.5 and pH > In pH viz. 9.87. Noticeably, the amount organic pollutant decomposed with respect to time is more at a lower pH when compared to the other cases. The time taken by $\text{SnS}_2/\text{KNbO}_3$ in degrading the same amount of dye as SnS_2 is lesser. Hence, it is a better photocatalyst than SnS_2 .

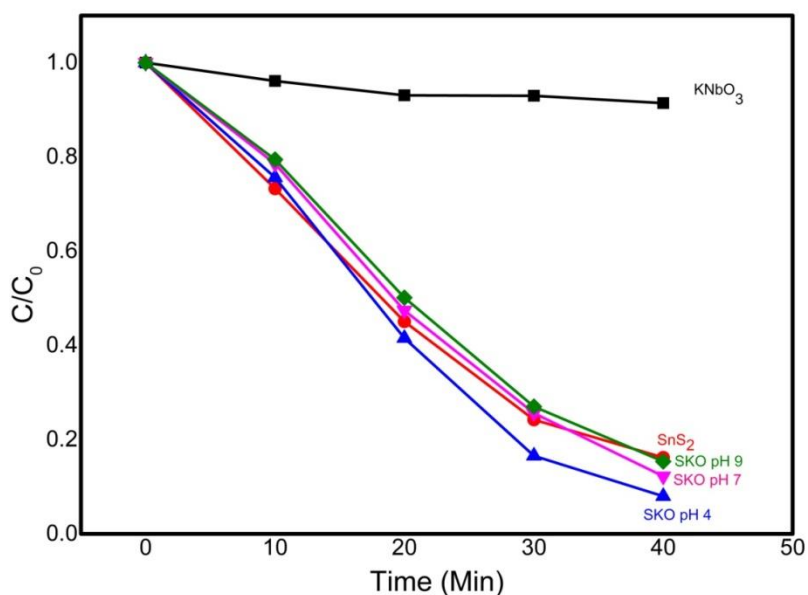


Figure 32: Degradation profiles of IC by $\text{SnS}_2/\text{KNbO}_3$ at different pH

When the photocatalyst $\text{SnS}_2/\text{KNbO}_3$ was subjected to attain adsorption/desorption equilibrium in the dark in the dispersed solution with IC, the surface electrons from the

heterostructure eventually transfer to the dye. Additionally, when the catalysts are subjected to visible-light driven irradiation with light energy approximately equal to their bandgap, it leads to excitation of electrons (e^-) in the valence band (VB) to conduction band (CB) leaving the same number of holes (h^+) in the VB at the same time. [21]

2.3 Conclusion:

Tin disulphide was investigated towards the application of photocatalysis under visible light using a metal halide lamp. SnS₂ being an-n-type semiconductor, it was coupled with a p-type semiconductor to enhance the photocatalytic ability. Hence, a perovskite p-type semiconductor KNbO₃ was chosen and engineered it to a heterostructure. This report has a collective data of pXRD, SEM, EDS, DRS supporting the existence of this heterostructure. But, in order to enhance the degradation ability of the catalyst and other applications like water splitting, furthermore optimization has to be done. Mainly, the *in situ* growth of SnS₂ over KNbO₃ and the morphology of the heterostructure. The degradation profiles of Indigo carmine were evaluated by SnS₂/KNbO₃ and its precursors, at various pH, proving an improvement in the degradation ability.

References:

1. Patzke, G. R.; Zhou, Y.; Kontic, R.; Conrad, F. Oxide Nanomaterials: Synthetic Developments, Mechanistic Studies, and Technological Innovations. *Angew. Chem., Int. Ed.*, 50, **2011**, 826
2. Tauc, J. Optical Properties and Electronic Structure of Amorphous. *Mater. Res. Bull.* **1968**, 3, 37.
3. Y.C. Zhang et al. Size-controlled hydrothermal synthesis of SnS₂ nanoparticles with high performance in visible light-driven photocatalytic degradation of aqueous methyl orange/ *Separation and Purification Technology* 81, **2011**, 101–107.
4. N.M. Julkapli, S. Bagheri, S.A. Hamid; Recent Advances in Heterogeneous Photocatalytic Decolorization of Synthetic Dyes; *the Scientific World Journal* **2014**, Article ID 692307.
5. S. Bae, S. Kim, W. Choi. Dye decolorization test for the activity assessment of visible light photocatalysts: Realities and limitations/ *Catalysis Today* 224 (**2014**) 21–28.
6. W.X.Li; Photocatalysis of Oxide Semiconductors. *Journal of the Australian Ceramic Society* 49[2], **2013**, 41 – 46.
7. S. Mandalidis, J.A. Kalomiros, K. Kambas, A.N. Anagnostopoulos. Optical investigation of SnS₂ single crystals. *J. Mater. Sci.* 31 (**1996**) 5975.
8. K.T. Ramakrishna Reddy, G. Sreedevi, K. Ramya, R.W. Miles. Physical Properties of Nano-crystalline SnS₂ Layers Grown by Chemical Bath Deposition. *Energy Procedia*, 15 (**2012**) 340 – 346.
9. Y Sun, S. Gao, F. Lei, Y. Xie. Freestanding Tin Disulfide Single-Layers Realizing Efficient Visible-Light Water Splitting. *Angew. Chem. Int. Ed.* **2012**, 51, 8727 –8731.
10. J. Wang, X. Li, X. Li, J. Zhub, H. Li. Mesoporous yolk–shell SnS₂–TiO₂ visible photocatalysts with enhanced activity and durability in Cr(VI) reduction. *Nanoscale.* **2013**, 5, 1876–1.
11. Shinri Sato. Photo-Kolbe Reaction at Gas-Solid Interfaces. *J. Phys. Chem.* **1983**, 87, 3531-3537.
12. M. Vautier, C. Guillard, J.M. Herrmann. Photocatalytic Degradation of Dyes in Water: Case Study of Indigo and of Indigo Carmine. *Journal of Catalysis*, 201, 46–59 (**2001**).
13. S. Greenwald, J.S. Smart. Deformations in the Crystal Structures of Anti-ferromagnetic Compounds. *Phys. Rev.* 82 (**1951**) 113.

14. M.E. McHenry, D.E. Laughlin, Nano-scale materials development for future magnetic applications *Acta Mater.* 48 (2000) 223.
15. D. R. Modeshia, R. I. Walton. Solvothermal synthesis of perovskites and pyrochlores: crystallisation of functional oxides under mild conditions. *Chem. Soc. Rev.*, 2010, 39, 4303– 4325.
16. Bullis, Kevin. A Material That Could Make Solar Power Dirt Cheap. *MIT Technology Review.* 2013.
17. G.K.L. Goh, F.F. Lange, S.M. Haile, C.G. Levi. Hydrothermal synthesis of KNbO₃ and NaNbO₃ powders. *J. Mater. Res.*, Vol. 18, No. 2, 2003.
18. Patzke, G. R.; Zhou, Y.; Kontic, R.; Conrad, F. Oxide Nanomaterials: Synthetic Developments, Mechanistic Studies, and Technological Innovations. *Angew. Chem., Int. Ed.*, 50, 2011, 826
19. Murphy A. B., “Solar Energy Materials and Solar Cells” 2007, 91, 1326.
20. J. Li, F. Meng, S. Suri, W. Ding, F. Huang, N. Wu. Photoelectrochemical performance enhanced by a nickel oxide–hematite p–n junction photoanode. *Chem. Commun.*, 2012, 48, 8213-8215.
21. Y. Zheng, L. Zheng, Y. Zhan, X. Lin, Q. Zheng, K. Wei. Ag/ZnO Heterostructure Nanocrystals: Synthesis, Characterization, and Photocatalysis. *Inorg. Chem.* 2007, 46, 6980–6986.
22. M. Niu, F. Huang, L. Cui, P. Huang, Y. Yu, Y. Wang. Hydrothermal Synthesis, Structural Characteristics, and Enhanced Photocatalysis of SnO₂/α-Fe₂O₃ Semiconductor Nanoheterostructures. *Nanoscale*, 2015, 7, 3117–3125.
23. W. Xu, M. Li, X. Chen, J. Zhao, R. Tan, R. Li, J. Li, W. Song; Synthesis of hierarchical Sn₃O₄ microflowers self-assembled by nanosheets *Materials Letters*, 120, (2014), 140–142.
24. A. Seko, A. Togo, F. Oba, I. Tanaka; Structure and Stability of a Homologous Series of Tin Oxides. *Phys. Rev. Lett.* 2008, 100, 045702.
25. M. Hara, T. Kondo, M. Komoda, S. Ikeda, K. Shinohara, A. Tanaka, J. N. Kondo, K. Domen. Cu₂O as a photocatalyst for overall water splitting under visible light irradiation. *Chem. Commun.*, 1998.
26. J. Li, S.K. Cushing, J. Bright, F. Meng, T.R. Senty, P. Zheng, A.D. Bristow, N. Wu. Ag@Cu₂O Core-Shell Nanoparticles as Visible-Light Plasmonic Photocatalysts. *ACS Catal.*, 2013, 3 (1), 47–51.

27. M. Manikandan, P. Li, S. Ueda, G.V. Ramesh, R. Kodiyath, J. Wang, J. Ye, N. Umezawa, H. Abe. Photocatalytic Water Splitting under Visible Light by Mixed-Valence Sn_3O_4 . *ACS Appl. Mater. Interfaces*, **2014**, 6 (6), 3790–3793.
28. Huaming Yang, J. Ouyang, A. Tang, Y. Xiao, X. Li, Y. Yu. Electrochemical synthesis and photocatalytic property of cuprous oxide nanoparticles. *Materials Research Bulletin*, 41, 7, **2006**, 1310–1318.
29. Ryu, J.; Choi, W. Effects of TiO_2 Surface Modifications on Photocatalytic Oxidation of Arsenite: The Role of Superoxides. *Environ. Sci. Technol.* **2004**, 38, 2928.
30. Y. Zheng; L. Zheng; Y. Zhan; X. Lin; Q. Zheng. Ag/ZnO Heterostructure Nanocrystals: Synthesis, Characterization and Photocatalysis. *Inorg. Chem.* **2007**, 46, 17.
31. G. Chen, S. Ji, Y. Sang, S. Chang, Y. Wang, J. Claverie, H. Liu, G. Yu. Synthesis of scaly $\text{Sn}_3\text{O}_4/\text{TiO}_2$ nanobelt heterostructures for enhanced UV-visible light photocatalytic activity. *Nanoscale*, **2015**, 7, 3117-3125.
32. S.S. Wilson, J.P. Bosco, Y. Tolstova, G.W. Watson, H.A. Atwater. Interface stoichiometry control to improve device voltage and modify band alignment in ZnO/Cu₂O heterojunction solar cells. *Energy Environ. Sci.*, **2014**, 7, 3606-3610.
33. Y.P. Yuan, L.W. Ruan, J. Barber, S. Chye, J. Loo, C. Xue. Hetero-nanostructured suspended photocatalysts for solar-to-fuel conversion. *Energy Environ. Sci.*, **2014**, 7, 3934–3951.
34. X. Li, P. Liu, Y. Mao, M. Xing, J. Zhang. Preparation of homogeneous nitrogen-doped mesoporous TiO_2 spheres with enhanced visible-light photocatalysis. *Applied Catalysis B: Environ.*, 164, **2015**, Pages 352-359.
35. G. Colón, M. Maicu, M.C. Hidalgo, J.A. Navío. Cu-doped TiO_2 systems with improved photocatalytic activity. *Applied Catalysis B: Environ.*, 67, 1–2, **2006**, 41–51.
36. Y. Xu, M.A.A. Schoonen. The absolute energy positions of conduction and valence bands of selected semiconducting minerals. *American Mineralogist*, 85, 543–556, **2000**.
37. P. Bernasconi, I. Biaggio, M. Zgonik, P. Günter. Anisotropy of the Electron and Hole Drift Mobility in KNbO_3 and BaTiO_3 . *Physical Rev. Lett.* **1997**, 78, 106-109.